

1 **Ex Vivo Validation of Six FDA-Approved Non-Receptor Tyrosine Kinase**
2 **Inhibitors (NRTKIs) as Antivirals to Pandemic and Seasonal Influenza A**
3 **Viruses**

4
5 Robert Meineke¹, Sonja Stelz¹, Maximilian Busch¹, Christopher Werlein², Mark Kühnel^{2,3},
6 Danny Jonigk^{2,3}, Guus F. Rimmelzwaan¹, Husni Elbahesh^{1,✉}

7
8
9 ¹ Research Center for Emerging Infections and Zoonoses (RIZ), University of Veterinary
10 Medicine (TiHo), Bünteweg 17, 30559 Hannover, Germany

11 ² Department of Pathology, Hannover Medical School (MHH), Carl-Neuberg-Straße 1,
12 30625 Hannover, Germany

13 ³ Member of the German Center for Lung Research (DZL), Biomedical Research in
14 Endstage and Obstructive Lung Disease Hannover (BREATH)

15
16
17 **Running Title: NRTKIs are effective influenza antivirals**

18
19
20
21
22 ✉ **Correspondence:** Husni.Elbahesh@tiho-hannover.de

23

24 **ABSTRACT**

25 Influenza viruses are important respiratory pathogens that cause substantial morbidity
26 and mortality annually. In addition to seasonal influenza outbreaks, new emerging
27 influenza A viruses (IAV) can cause pandemic influenza outbreaks. Apart from effective
28 vaccines, there is a need for better treatment options to combat infections with these
29 viruses when vaccines are not available or show reduced efficacy (e.g., in
30 immunocompromised patients). The limited range of licensed antiviral drugs and
31 emergence of drug-resistance mutations highlight the need for novel intervention
32 strategies like host-targeted antivirals. Repurposing FDA-approved kinase inhibitors may
33 offer a fast-track for a new generation of host-targeted antivirals. Small molecule kinase
34 inhibitors (SMKIs) can inhibit replication of viruses and improve survival *in vivo*; however,
35 no SMKI has been approved for clinical use against IAV infections. In the present study,
36 we tested eight non-receptor tyrosine kinase-inhibitors (NRTKIs) used to treat cancer and
37 autoimmune diseases for their antiviral potential. Six of those potently inhibited virus
38 replication ($\geq 1,000$ -fold) in A549 cells infected with either A(H1N1)pdm09 or seasonal
39 A(H3N2) strains. These compounds were validated in a biologically relevant *ex vivo*
40 model of human precision-cut lung slices (hPCLS) to provide proof of principle and show
41 efficacy against contemporary seasonal and pandemic IAVs. We identified the steps of
42 the virus infection cycle affected by these inhibitors and assessed the effect of these
43 NRTKIs on the host response. Considering their established safety profiles, our studies
44 show that the use of these NRTKI shows promise and warrants further development as
45 an alternative strategy to treat influenza virus infections.

46

47 INTRODUCTION

48 Influenza viruses are an important cause of respiratory tract infections in humans and
49 are responsible for substantial annual morbidity and mortality, especially in individuals at
50 high risk, like older adults or immunocompromised patients. The most important
51 preventive measure to protect humans from influenza virus infections is vaccination.
52 Currently used vaccines mainly aim at the induction of virus neutralizing antibodies to the
53 viral hemagglutinin (HA). For vaccines to be effective they need to antigenically match
54 the circulating strains.¹⁻³ Due to a lack of proof-reading activity of their RNA-dependent
55 RNA polymerase (RdRp), influenza viruses can accumulate mutations that lead to
56 antigenic drift and allow them to evade recognition by virus-neutralizing (VN) antibodies
57 induced by previous infections or vaccinations. These antigenic changes also necessitate
58 annual update of influenza vaccines against seasonal influenza⁴. Moreover, emergence
59 of novel influenza viruses that arise through genetic reassortment after interspecies
60 transmission. Emergence of these viruses in human populations that largely lack VN
61 antibodies can result in pandemic outbreaks. At the early stages of a pandemic, effective
62 vaccines are not readily available, as was the case during the pandemic of 2009 caused
63 by swine-origin A(H1N1) influenza A viruses (IAVs).

64 In the absence of efficacious vaccines, virus-targeted antivirals can offer some
65 protection if administered within the therapeutic window. Until recently, influenza antivirals
66 were comprised of two classes, Adamantanes that target the viral M2 ion channel protein
67 and neuraminidase inhibitors (NAI). Due to almost ubiquitous resistance found in currently
68 circulating strains, Adamantanes have been rendered ineffective and are no longer used
69 in clinical practice⁵. The levels of currently circulating viruses that carry resistance

70 mutations to NAIs (such as oseltamivir) isolated from otherwise healthy individuals is only
71 ~4-5%⁶. A more recent strategy has been to target the influenza polymerase proteins,
72 with Favipiravir (T705), Baloxavir and Pimodivir targeting the viral PB1, PA and PB2
73 polymerase subunit proteins, respectively being the most widely used antivirals. All seem
74 to inhibit viruses that are resistant to Adamantanes and NAIs^{7,8}. In 2018, Baloxavir was
75 approved for the treatment of acute and “uncomplicated” influenza infections in the United
76 States^{9,10}. Surprisingly, Uehra et al. found that even in otherwise healthy adults and
77 adolescents the emergence of strains carrying Baloxavir resistance mutations was as
78 high as ~10% and could potentially be higher in immunocompromised patients^{11,12}.

79 The sustained circulation of virus variants resistant to current antivirals and the low
80 genetic barrier to achieve resistance highlight the need for host-targeted therapeutics;
81 that do not suffer from these limitations. Given that all viruses rely on host-cellular
82 machinery for replication at every step of their life cycle, several host proteins have been
83 shown to be required for efficient viral replication and pathogenesis¹³⁻¹⁷. Host kinases
84 link a myriad of signaling pathways used by viruses; and as such, they offer attractive
85 targets for potential host-directed therapeutics against infections by several viruses
86 including influenza viruses^{13,14,18}. Host kinases catalyse phosphorylation of lipids or
87 proteins, at either tyrosine or serine/threonine residues that not only serves to relay and
88 amplify cell signaling, but phosphorylation can also lead to conformational changes in
89 proteins that facilitate protein-protein interactions^{19,20}.

90 Although the human kinome consists of more than 550 kinases, currently available
91 kinase inhibitors only target ~10% of kinases and are primarily used to treat cancers²¹⁻
92 ²⁵. To date, only 62 small-molecule kinase inhibitors (SMKIs) have been FDA-approved

93 and the majority of these target tyrosine kinases ²⁶. Non-receptor tyrosine kinases
94 (NRTKs) are cytoplasmic or membrane-anchored kinases that closely associate with
95 cellular receptors or receptor complexes to mediate outside-in signaling ²⁶. NRTKs like
96 most kinases contain a catalytic kinase domain, as well as several protein-protein
97 interaction motifs (e.g., SH2, SH3, PH domains, etc.) necessary to relay cell signals.
98 NRTKs include Abl, FAK, JAK, Src and BTK, all of which have been reported to play a
99 role in IAV infections. Previous studies have demonstrated that NRTK inhibitors (NRTKIs)
100 can modulate pro- and anti-viral signaling *in vitro* and result in reduced viral pathogenesis
101 and increased survival *in vivo* ^{13,16,27-32}. However, no NRTKIs or SMKIs have been
102 approved for clinical use against influenza. In the present study, we characterized the
103 effect of eight currently available and FDA-approved NRTKIs on IAV replication, six of
104 which were validated using a biologically relevant *ex vivo* model of human precision-cut
105 lung slices (hPCLS). hPCLS maintain near-native structural integrity of lung tissues that
106 allow complex and 3D cell-cell interactions of epithelial cells, mesenchymal tissue as well
107 as the vascular compartment; thereby, offering an advantage over cultured epithelial
108 monolayers ³³⁻³⁵. We also identify which steps of the virus infection cycle are affected by
109 specific NRTKIs; thereby providing insights into potential mechanisms of action in the
110 context of influenza virus infections.

111

112 **RESULTS**

113 **NTRKI treatment inhibits IAV replication *in vitro***

114 To identify non-toxic concentrations of our inhibitors, we used the CellTiter-Glo (CTG)
115 assay in which cell-viability is based on ATP content in healthy cells. We identified

116 concentrations that resulted in cell viability $\geq 90\%$ relative to mock-treated cells (cells
117 treated with 0.1% DMSO). The highest concentration with $\geq 90\%$ relative viability was
118 defined as the 1x concentration ($[1x]_{\max}$) (**Fig. 1/Table 1**).

119 Next, we determined the effect of eight NRTKIs on influenza A virus replication. A549
120 cells were infected with either pandemic A(H1N1)pdm09 strain A/Netherlands/602/09
121 (NL09) or seasonal A(H3N2) strain A/Netherlands/241/11 (NL11) at a multiplicity of
122 infection (MOI) of 1 in the presence or absence of $[1x, 0.5x$ and $0.25x]_{\max}$ concentrations
123 of the respective inhibitors following inoculation. Culture supernatants were collected at
124 2, 24, 48, and 72 hours post infection (hpi) and virus titers were determined by median
125 tissue culture infectious dose (TCID₅₀) assay. We observed a dose-dependent reduction
126 of viral titers by six of the eight inhibitors with at least one of the concentrations ranging
127 from 2- to 1,000-fold (**Fig. 2A**) reduction of virus titers. As visualized by the heatmap (**Fig.**
128 **2B**), there was variability in both magnitude and duration of the reduction of virus titers,
129 and in general, the effect was more pronounced in NL11 (H3N2) infected cells than NL09
130 (pH1N1). Although we observed only a transient reduction at 24 hpi with Tofacitinib (TF)
131 (JAK1/2/3 inhibitor)³⁶, we did not observe any significant reduction with Ruxolitinib (RX)
132 (JAK1/2 inhibitor)³⁷. The highest and most sustained level of reduction was observed with
133 Nilotinib (NI) (Abl/PDGFRa inhibitor)^{38,39}: $>1,000$ -fold (3-log_{10}) reduction. Bosutinib (BO)
134 (Abl/Src/Btk inhibitor)^{40,41} and Saracatinib (SA) (Src inhibitor)⁴² also showed marked
135 inhibition (SA ~ 5 - to 25-fold; BO ~ 10 - to 1,000-fold). Acalabrutinib (AC) (Btk inhibitor)^{43,44}
136 had very little effect on NL09 replication but showed a greater and more sustained
137 inhibition (5- to 25-fold) of NL11 replication at the higher concentrations (0.25 and 0.5
138 μM). Similarly, Ibrutinib (IB) (Btk/EGFR inhibitor)^{45,46} had little to no effect on NL09

139 replication but a more appreciable and sustained (5- to 100-fold) reduction, especially at
140 the highest concentration used (0.5 μ M) of NL11 replication. Defactinib (DF) (FAK/Pyk2
141 inhibitor)⁴⁷ treatment resulted in robust reduction in viral titers (10- to 1,000-fold) in both
142 NL09 and NL11 at the higher concentrations (2.5 and 5.0 μ M). In NL09 infected cells, the
143 reduction was more robust at earlier time-points (24 and 48 hpi), but in NL11 infected
144 cells a larger reduction was observed at 24 and 72 hpi than at 48 hpi.

145

146 **NRTKIs affect IAV infectivity and cell viability during IAV infection**

147 Host-targeted inhibitors can influence virus yield by affecting infectivity through effects
148 on viral entry, RNA replication, increased host antiviral responses as well as impacting
149 the viability of infected cells. To assess the effect of NRTKIs on viral infectivity and cellular
150 viability, we used immunofluorescence microscopy to determine the number of infected
151 cells as well as the total number of cells. A549 cells were infected with either NL09 or
152 NL11 (MOI=1) in the presence of NRTKIs [0.5x]_{max}, fixed at 48 hpi and stained to detect
153 virus and nuclei (**Fig. 3A**). Surprisingly, treatment with most inhibitors resulted in a
154 significant increase in infectivity despite the reduction in viral titers observed in **Fig. 2**. We
155 observed robust increases in relative infectivity in cells treated with TF (NL09=217%,
156 NL11=112%), RX (NL09=203%, NL11=116%) and DF (NL09=180%, NL11=139%). We
157 only observed a marginal increase in relative infectivity (~105%) in cells treated with either
158 BO or NI in both NL09- and NL11-infected cells. We observed a marked decrease in
159 relative infectivity in cells treated with AC (NL09=78%, NL11=74%) and SA (~90% for
160 both NL09 and NL11). Interestingly, we observed opposite effects on NL09 (increased)-

161 and NL11 (decreased)-infected cells following treatment with IB (NL09=116% vs
162 NL11=91%) (**Fig. 3B**).

163 Next, we determined whether the reduction in titers was the result of reduced cell
164 viability using the CellTiter Glo assay described above. Although at the NRTKI
165 concentrations used $[0.5x]_{\max}$ we observed less than 5% cytotoxicity in mock-infected
166 cells, IAV-infection led to synergistic cytotoxicity and decreased relative viability when
167 treated with TF (NL09=40%, NL11=63%), RX (NL09=66%, NL11=89%) or DF
168 (NL09=84%, NL11=92%). However, cell viability was increased by treatment of IAV-
169 infected cells with AC (NL09=112%, NL11=109%), IB (NL09=102%, NL11=109%) BO
170 (NL09=111%, NL11=114%), NI (NL09=110%, NL11=110%) or SA (NL09=150%,
171 NL11=127%) (**Fig. 3B**). Taken together, our data suggest that decreased infectivity or
172 cell viability alone do not account for the NRTKI induced reduction in viral titers we
173 observed.

174

175 **The antiviral effect of NRTKIs is MOI-independent**

176 Given the viability data and the limited reduction in viral titers above, we excluded RX
177 and TF from further analyses and focused on the remaining six NRTKIs for further
178 investigation. We assessed whether the inhibitory effects of NRTKIs we observed were
179 dependent on the infectious dose used. We infected A549 cells with either a high MOI
180 (MOI=3) or a low MOI (MOI=0.01) in the presence or absence of NRTKIs $[0.5x]_{\max}$.
181 Culture supernatants were collected at 2, 24, 48, and 72 hpi and virus titers were
182 determined by TCID₅₀ assay. As we previously observed, the effect on the seasonal H3N2
183 (NL11) strain was more pronounced compared to that on the pandemic H1N1 (NL09)

184 strain; presumably due to the faster growth kinetics of NL11 compared to NL09. However,
185 similarly to cells infected at MOI=1 (**Fig. 2**), NRTKI treatment of cells infected at either
186 high (3) or low (0.01) MOI resulted in viral titer reductions of at least 10-fold (1-log_{10}) (**Fig.**
187 **4**). Treatment with either DF, BO or NI had a larger impact on early (24 hpi) viral
188 replication, especially in NL11 infected cells. And although peak titers of untreated cells
189 infected with NL11 were similar at either MOI, cells infected at MOI=0.1 exhibited the
190 greatest reduction of $\sim 1,000$ -fold (3-log_{10}). Although AC, IB and SA treatment had less of
191 an impact on viral titers than DF, BO or NI, viral titer reductions were still up to 100-fold
192 (2-log_{10}) (**Fig. 4**).

193

194 **Human PCLS support robust IAV infection and confirm inhibitory effect of NRTKI** 195 **treatment**

196 We utilized human precision-cut lung slices (hPCLS) as a biologically relevant *ex vivo*
197 model that more faithfully represents lung tissues than either 2D monolayer cultures or
198 3D air-liquid-interface (ALI) cultures^{33,34}. Following hPCLS preparation, they were in
199 culture for up to 4 weeks; no gross alterations in cell type or morphology were observed
200 and cilia beating was observed in all used hPCLS (8 donors; n=24). We first sought to
201 identify an infectious dose to synchronize peak titers in hPCLS infected with either NL09
202 or NL11 as these two strains have different replication kinetics *in vitro*. hPCLS were
203 infected with 10^4 , 10^5 , or 10^6 TCID₅₀ / 200 μ L with either NL09 or NL11. To limit donor-
204 heterogeneity effects, we used hPCLS from 8 donors (n=24/virus). Culture supernatants
205 were collected and replenished at 2, 16, 24, 48, 72, 96, and 144 hpi and virus titers were
206 determined by TCID₅₀ assay using the collected supernatants. Interestingly, the 10^6 dose

207 yielded maximal titers that were lower than the other doses and were achieved by 24 hpi
208 with either strain. However, the highest peak titers were achieved at 48 hpi following
209 infection with either 10^4 or 10^5 doses of NL11, but only in the 10^5 dose of NL09 (**Fig. 5A**).
210 Based on these results the 10^5 dose was used in all our subsequent hPCLS infections.

211 Next, we determined the tolerability of hPCLS to our NRTKIs candidates. hPCLS were
212 treated with either the $[1x \text{ or } 10x]_{\max}$ (1x is highest non-toxic NRTKI concentration defined
213 using A549 cells). Culture supernatants were collected and replenished at 24, 48, 72, 96,
214 and 144 h. Lactate dehydrogenase (LDH) release into the culture supernatant due to loss
215 of plasma membrane integrity is an indicator for cytotoxicity. Using a bioluminescence
216 based LDH detection assay (LDH-Glo Cytotoxicity Assay), we quantified LDH released
217 into the collected supernatants following NRTKI treatment. As a positive control for
218 cytotoxicity, hPCLS were treated with 0.1% Triton-X 100; DMSO-treated hPCLS were
219 used as a vehicle control (**Fig. 5B**). Our cytotoxicity cut-off was 20% of the positive control
220 treatment; none of the NRTKIs surpassed this cut-off at $[1x]_{\max}$. However, $[10x]_{\max}$
221 concentrations of DF (50 μM), BO (50 μM) and SA (1.25 μM) showed significantly higher
222 cytotoxicity that was above the relative 20%-cutoff; therefore, only the 1x concentrations
223 of these NRTKIs were used in subsequent hPCLS experiments.

224

225 **NRTKIs inhibit *ex vivo* IAV infections**

226 Based on our *in vitro* data, we tested six NRTKIs (AC, BO, DF, IB, NI and SA) for their
227 antiviral potential. hPCLS from 3 donors (n=6/virus/condition) were infected with 10^5
228 TCID₅₀ of either NL09 or NL11 and then treated with NRTKIs (DF 5 μM ; AC 5 μM ; IB 5 μM ;
229 BO 5 μM ; NI 10 μM ; SA 0.125 μM). Culture supernatants were collected and replenished

230 from the same wells at 2, 12, 24, 48, 72, and 120 hpi and virus titers were determined by
231 TCID₅₀ assay. We observed a significant and robust reduction in viral titers of at least 10-
232 fold or 1-log₁₀ (DF treatment) to more than 1,000-fold or 3-log₁₀ (IB and NI treatments)
233 using all the NRTKIs (**Fig. 5C**). Moreover, unlike what we observed in A549 cells, NRTKI-
234 mediated IAV inhibition was observed as early as 12 hpi and maintained at 120 hpi;
235 beyond the times when peak titers were achieved (48-72 hpi) (**Fig. 5C**).

236 Next, we assessed the effect of NRTKI treatment on viral spread and associated
237 damage to the epithelium. Considering we did not observe significant differences in titer
238 reductions between NL09 and NL11, only data for NL11 is shown (**Fig. 5D**). At 120 hpi,
239 mock- and IAV-infected hPCLS (n=3/virus/condition) were fixed and paraffin-embedded.
240 Tissue sections (2 μm thick) were cut, stained and immunoprobed. H&E staining indicated
241 that no gross alterations in cell composition or the epithelium were observed in mock-
242 infected cells indicating viability of hPCLS. Typical morphological changes associated
243 with IAV infections were observed. Using consecutive sections from those H&E stained,
244 we detected the viral spread using antibodies to IAV-NP (**Fig. 5D**). We observed specific
245 staining of viral antigen in all observed cell-types including type I/II pneumocytes and
246 endothelial cells. Additionally, staining intensity and quantity was reduced in NRTKI
247 treated hPCLS compared to untreated hPCLS.

248 We carried out semiquantitative analysis of the acquired images to compare the effect
249 of the inhibitors on viral spread in hPCLS with variable tissue density. IAV-NP signal was
250 normalized to H&E staining of the respective regions in consecutive tissue section.
251 Treatment with DF, AC, BO and SA significantly reduced the infectivity by > 50%, whereas
252 treatment with IB and NI had limited effects on infectivity (**Fig. 5E**).

253

254 **Stability of NRTKI inhibition**

255 Host-directed antivirals/therapeutics are thought to have a higher barrier of resistance
256 than their virus-targeted counterparts. To determine the stability of the antiviral effect of
257 our NRTKIs, we phenotypically assessed the possibility of the emergence of resistant
258 escape variants ^{48,49}. We passaged both NL09 and NL11 viruses (MOI=0.001) in the
259 presence of NRTKIs [$1x$]_{max} in MDCK cells for 5 passages. Untreated virus stocks were
260 also passaged as a control. At each passage, virus supernatant was quantified and used
261 to inoculate the next passage at MOI=0.001 again. In untreated passages, the virus titers
262 for both NL09 and NL11 was similar from passages 1 to 5 but were significantly lower in
263 all treated passages (**Fig. 6A**); the reduction was comparable to what we originally
264 observed in A549 cells. The viral titers were stable at all passages indicating that no
265 resistance mutations were acquired. To rule out the possibility that the NRTKIs directly
266 interact with the virion and inhibit its attachment or entry, we pre-incubated virus stocks
267 with NRTKIs [$1x$]_{max} for 2 h then diluted the virus stocks 1:1000 to minimize the effects on
268 host cells, and infected A549 cells. At 72 hpi, culture supernatants were collected and
269 virus titrated by TCID₅₀ assay. As expected, pre-treatment of virus with NRTKIs had no
270 effect on viral titers, indicating that the observed effects are due to host-cell effects (**Fig.**
271 **6B**).

272

273 **Selected NRTKIs inhibit viral entry**

274 Kinases regulate every step of the infection cycle and a single kinase can affect
275 multiple steps ^{28,29}. We first assessed whether our NRTKIs impaired viral entry. A549 cells

276 were pretreated for 2 h, then chilled on ice for 15 min and infected at a high MOI (MOI=10)
277 on ice for 30 min to synchronize the infection and allow binding of the virus to cell surface
278 receptors but not trafficking of virions. Unbound and non-internalized virus was washed
279 away with room temperature PBS. Cells were then incubated with prewarmed infection
280 media in the presence or absence of NRTKIs. At 0.5 hpi, cells were fixed, stained to detect
281 viral NP, F-actin and nuclei and analyzed by confocal microscopy. We observed
282 significant retention at the membrane and periphery of the cell following DF and IB
283 treatment (**Fig. 7**). Surprisingly, no virus was detected in response to BO treatment and
284 the F-actin network was not detectable. Given the sustained viability of BO-treated cells,
285 it is likely that the altered actin dynamics are well tolerated. No significant changes were
286 detectable in AC, NI or SA treated cells suggesting these inhibitors did not affect viral
287 entry under our tested conditions (**Fig. 7**).

288

289 **NRTKIs exert differential effects on IAV polymerase activity**

290 Next, we assessed the effect of our NRTKIs on viral RNA replication using the pPOLI-
291 358-FFLuc reporter plasmid, which encodes a firefly luciferase gene under control of the
292 viral nucleoprotein (NP) promoter. In this system, luciferase activity is a surrogate for viral
293 polymerase activity⁵⁰⁻⁵². A549 cells were transfected with pPOLI-358-FFLuc and
294 pmaxGFP plasmids (transfection control). At 24 hpt, cells were either infected with NL09
295 or NL11 at MOI=1 in the presence or absence of indicated NRTKIs at either [0.5x or
296 1x]_{max}. At 48 h post-transfection (hpt) (~24 hpi), luciferase activity was measured,
297 normalized to GFP expression (MFI) and represented as relative of untreated infected
298 cells. We observed a significant reduction in polymerase reporter activity in response to

299 AC (NL11 only), IB (NL09 only), BO, NI and SA (NL11 only) (**Fig. 8A, left panel**). Although
300 the magnitude of reduction was higher in NL09-infected than NL11-infected cells, a
301 significant reduction was more readily observed in NL11 infected cells at a lower NRTKI
302 concentration compared to NL09 infected cells. DF also reduced reporter activity
303 (NL09=20%, NL11=13%), however this reduction was not statistically significant. At 24
304 hpi, a 3-fold increase in reporter activity could be observed in untreated NL11-infected
305 cells over untreated NL09-infected cells; this is in-line with faster replication kinetics of
306 NL11 compared to NL09 (**Fig. 8A, right panel**).

307 To better dissect the direct effect on viral RNA replication in the absence of
308 confounding factors due to NRTKI influences on viral entry and host responses, we
309 utilized an established minigenome system. A549 cells were transfected with pPOLI-358-
310 Ffluc and pmaxGFP plasmids and co-transfected with either NL09 or NL03-minigenome
311 plasmids that encode the viral NP, PA, PB1 and PB2 replication complex proteins. At 6
312 hpt, the indicated NRTKIs were added to the medium at either [0.5x or 1x]_{max}. At 30 hpt
313 (24 h of treatment), luciferase activity was measured, normalized and represented as
314 above. In this context, AC (NL09 only), IB, NI and SA treatments significantly reduced
315 polymerase activity (**Fig. 8B**). In contrast to what we observed in infected cells, the
316 magnitude of reduction in polymerase activity was comparable in NL09- and NL11-
317 minigenome transfected cells. Interestingly, polymerase activity was significantly higher
318 in untreated H1N1 (NL09) than H3N2 (NL03) minigenome-transfected cells.

319

320 **NRTKIs do not affect innate immune responses during IAV infections**

321 Given that our NRTKIs reduced viral titers by affecting either viral entry or replication,
322 we speculate whether these effects were coupled to altered innate immune signaling.
323 Activation of STAT3 by IFN type-I, -II, and -III as well as by interleukins results in
324 phosphorylation of STAT3 at Y705. We assessed the level of pSTAT3 (pY705) in A549
325 cells infected with either NL09 or NL11 (MOI=1) in the presence or absence of NRTKIs
326 at $[1x]_{max}$. At 18 and 48 hpi, total proteins were isolated from whole cell lysates, separated
327 by SDS-PAGE and analyzed by immunoblotting. We observed a decrease in the relative
328 pSTAT3/total STAT3 ratio in untreated NL09-infected cells at 18 and 48 hpi (**Fig. 9A**)
329 compared to mock-infected cells (18 h = 159%, 48 h = 225%). This reduction was less
330 striking in NL11-infected cells (**Fig. 9B**). Only DF treatment resulted in a significant
331 reduction of pSTAT3 relative to untreated infected cells (NL09 = 5% to 8%, NL11 = 5%
332 to 14% of untreated). None of the other NRTKIs showed a significant effect.

333 Phosphorylation of NFkB p65 (pNFkB) at S536 results in activation of the NFkB
334 pathway. We did not detect an increase in the relative pNFkB/total NFkB ratio in NL09-
335 infected cells compared to mock-infected cells at either 18 or 48 hpi following treatment
336 with any of the NRTKIs (**Fig. 10A**). In contrast, we observed a slight increase in the
337 pNFkB/total NFkB ratio in untreated NL11-infected cells at 18 and 48 hpi (**Fig. 10B**)
338 compared to mock-infected cells (18 h = 75%, 48 h = 89%). Although we did observe a
339 reduction in NFkB activation following DF treatment of NL11-infected cells (18 h = 64%,
340 48 h = 68% of untreated), this reduction was not statistically significant. We next
341 confirmed that NFkB signaling is not impaired in our system. Mock-infected cells were
342 treated with high-molecular weight poly(IC), a synthetic dsRNA, at either 50 or 200 ng/ml.
343 Following infection of cells with NL09 or NL11 (MOI=1), cells were treated with 200 ng/ml

344 poly(IC). At 18 and 48 hpi, total proteins were isolated from whole cell lysate, separated
345 by SDS-PAGE and analyzed by immunoblotting. At 18 hpi, the relative pNFkB/total-NFkB
346 ratio significantly increased in response to poly(IC) stimulation with both low and high
347 concentrations (~7-fold relative to untreated 18 h mock) (**Fig. 10C**). Similarly, poly(IC)
348 treatment of NL09 or NL11 infected cells had a robust increase in NFkB activation (NL09
349 = ~10-fold, NL11 = ~17-fold relative to untreated 18 h mock) (**Fig. 10C**). By 48 hpi, the
350 observed NFkB activation was back to untreated-levels in mock, NL09 and NL11 infected
351 cells. These data further support our results that IAV-induced NFkB activation is limited
352 later during infection; likely suppressed by the viral NS1 (**Fig. 10C**).

353

354 **DISCUSSION**

355 Despite their clear susceptibility to rapidly arising resistance mutations, virus-targeted
356 antivirals are still the only available class of antivirals against respiratory viruses such as
357 influenza. In this study, we screened FDA approved SMKIs currently in clinical use
358 against cancers and autoimmune diseases for their antiviral potential against IAV
359 infections. Six of the eight NRTKIs we tested showed a potent inhibition of pandemic
360 A(H1N1)pdm09 and seasonal A(H3N2) IAV strains with little to no impact on cell viability
361 *in vitro*. We further validated these NRTKI candidates using a faithful *ex vivo* model of
362 human PCLS. We identified the step(s) of the viral replication cycle affected by each
363 compound. In doing so, we provide valuable information on the interplay of signaling
364 pathways regulating these steps and the likely kinases involved.

365 Kinase dysfunction often leads to malignancies and tumor immune evasion.
366 Therefore, kinases have been heavily targeted for cancer treatments using selective

367 inhibitors²⁶. At the molecular level, most kinases regulate signaling pathways via catalytic
368 and/or protein-scaffolding activities. Phosphorylation often triggers changes in protein
369 conformation, enzymatic activity or subcellular localization; all of which allow fine-tuning
370 of protein-protein interactions to mediate stimuli-specific responses⁵³. Indeed, host
371 kinases play a critical role in IAV entry, replication, and release as well as viral
372 evasion/suppression of hosts immune responses. These processes often require
373 phosphorylation of viral proteins by mostly unidentified kinases⁵⁴⁻⁶⁵.

374 We carried out our initial screening using A549 cells (ATII lung adenocarcinoma);
375 however, due to potential biases associated with aberrant expression and kinase activity
376 of cancerous cell-lines, we validated candidate NRTKIs using human PCLS (hPCLS).
377 Unlike 2D monolayers or 3D well-differentiated air-liquid interface (ALI) cultures, PCLS
378 preserve the native lung tissue architecture, cellular composition including endothelial,
379 ATI and ATII epithelial cells, fibroblasts and maintain the native extracellular matrix³³⁻³⁵.
380 Moreover, the tissue tropism and infectivity of certain viruses may not be accurately
381 represented *in vitro* due to the absence of relevant cell-cell interactions that can influence
382 infectibility and host responses⁶⁶. Accordingly, we observed a similar discrepancy in
383 which the strain-dependent differences observed in NRTKI-treated A549 cells were not
384 observed in hPCLS, suggesting that the variations between IAV strains in A549 might be
385 an *in vitro* artifact. Moreover, we observed a wide tissue tropism in hPCLS which suggests
386 that while ATII cells may support more efficient infection, other cell-types of the lung are
387 readily infectible as well. Nevertheless, we observed robust viral titer reductions in both
388 systems following NRTKI treatment that were not readily explained by a reduction in
389 infectivity or cell viability. Considering that the smallest reductions in viral titers were

390 observed following Defactinib (DF) < Acalabrutinib (AC) < Saracatinib (SA) < Bosutinib
391 (BO) treatment, hPCLS infectivity was reduced by ~50% by each of those NRTKIs.
392 Similarly, Ibrutinib (IB) and Nilotinib (NI) had the largest effect on viral titers but increased
393 infectivity (NI:~22%, IB=~7%). Together our data suggest that reduction in infectivity of
394 either A549 cells or hPCLS does not fully account for the potent reduction in viral titers
395 and supports a *bona fide* effect of NRTKIs on either viral entry or RNA replication.

396 Although there is a growing body of *in vitro* and *in vivo* evidence to support the use of
397 kinase inhibitors, not a single SMKI has been approved or licensed for the treatment of
398 influenza virus infection so far ^{4,13,14,17,60}. SMKI selectivity remains a contentious topic and
399 has been a hurdle to the pursuit of kinase inhibitors as antivirals. Assumptions made
400 regarding “off-target effects” are attributed to changes in phosphorylation or activation of
401 proteins/pathways besides the intended target. While compounds still in the pre-clinical
402 development phase require target validation, the selectivity of compounds in clinical use
403 has been heavily investigated ^{26,67-69}. The ever-expanding kinase-substrate interaction
404 map highlights the extensive crosstalk between signaling pathways. Therefore, inhibition
405 of an “off-target” kinase or pathway, cannot be oversimplified and attributed to promiscuity
406 of the SMKI in question; rather it is more likely evidence of an interaction between the
407 intended target and the affected “off-target” signaling node. Two seminal studies
408 collectively examined selectivity of over 170 SMKIs against more than 440 kinases,
409 covering ~80% of the human kinome. In the first study, Davis et al. compared inhibitor-
410 kinase binding affinities, whereas Anastassiadis et al. used functional kinase inhibition
411 assays in the second study. They determined that while classes of SMKIs may inhibit
412 multiple kinases within a single subfamily, inhibitors are selective against kinases outside

413 that subfamily ^{68,69}. However, a limitation of those studies is that they were carried out
414 using truncated or fused recombinant proteins that may adopt altered conformations in
415 the absence of regulatory domains (i.e., regulatory subunit of PI3K) or binding partners
416 that may influence availability of substrate or ATP binding sites ²⁶. Moreover, selectivity
417 of clinically approved SMKIs was validated by super resolution microscopy (dSTORM) to
418 show the superior specificity and selectivity of fluorescently labeled SMKIs like Gefitinib
419 (EGFR inhibitor), over either a fluorescently labeled EGF ligand or an EGFR monoclonal
420 antibody ⁷⁰.

421 In addition to their therapeutic uses, kinase inhibitors are used as molecular beacons
422 to probe host signaling pathways and delineate how they are regulated by kinases. It is
423 not surprising that NRTKIs which target known effectors of IAV entry have a significant
424 effect on this step of the replication cycle. Indeed, we previously showed that targeting
425 FAK using the pre-clinical inhibitor Y15, led to inhibition of PI3K-mediated endosomal
426 trafficking of virions ²⁸. Using the FDA-approved FAK inhibitor DF, we saw comparable
427 effects on actin reorganization and viral entry as we previously observed using Y15 ²⁸.
428 This is consistent with the fact that the most prominent effect of DF on viral replication in
429 both A549 and hPCLS was at earlier time-points when reduction in viral entry may have
430 a larger impact than at later time-points. Indeed, we observed a reduction in infectivity in
431 response to DF treatment which is consistent with the observed reduction of viral entry.

432 Bruton's tyrosine kinase (BTK) activity regulates survival, proliferation and
433 inflammatory responses in B-cells, as well as epithelial cells ⁷¹. Cell-specific BTK isoforms
434 have recently been implicated in PI3K and PLC γ signaling that are either pro- or anti-
435 apoptotic ⁷². IB and AC are two high-affinity irreversible inhibitors of BTK; IB also inhibits

436 EGFR activity^{73,74}. IB treatment reduces excessive neutrophil infiltration, acute lung injury
437 (ALI) and subsequent ARDS; ultimately resulting in increased survival of mice severely
438 infected with IAV²⁷. Given that IB inhibits both EGFR and BTK whereas AC selectively
439 inhibits BTK, the IB-specific reduction in viral entry we observed, suggests this effect is
440 mediated largely through inhibition of EGFR signaling. This is consistent with IAV-induced
441 EGFR signaling which facilitates viral entry and activation of downstream pathways (Src,
442 PI3K and ERK) that promote efficient replication⁷⁵.

443 BO, along with NI and SA, are second-generation Src inhibitors. BO also inhibits Abl
444 kinase and to a lesser extent BTK. Src orchestrates signaling across multiple pathways
445 that regulate proliferation, survival, cell-cell communication, innate immune responses
446 and apoptosis²⁵. Growth factor RTKs like PDGFR and EGFR induce Src-mediated
447 activation of PI3K/AKT, Ras-Raf-MEK-ERK, FAK, and STAT3⁷⁶. Accordingly, Src plays
448 a mostly proviral role during IAV infections that is modulated by the viral NS1 protein^{13,77}.
449 In contrast, Abl's role in human IAV infections is not clear; however, Abl inhibition by some
450 avian IAVs results in significant pathology *in vitro* and *in vivo*^{78,79}. We observed a
451 significant reduction in viral titers following BO treatment of hPCLS and A549 cells which
452 also resulted in a stark reduction in viral entry, largely due to disruption of the actin
453 network. Despite the increase in cell viability during infection, we observed a complete
454 absence of detectible actin filaments suggesting either enhanced depolymerization of F-
455 actin or altered actin dynamics. Consequently, BO inhibition of Src activity can lead to
456 actin depolymerization due to retention of alpha and β -catenin at the cell membrane^{80,81}.

457 To dissect the effect of our NRTKIs on polymerase activity, we employed a
458 polymerase activity reporter system⁸². Interestingly, in the context of viral infections, we

459 detected higher polymerase reporter activity in NL11 (H3N2)-infected cells. In contrast,
460 significantly higher polymerase activity was detected using NL09 (H1N1) minigenome.
461 Faster kinetics may be more susceptible to NRTKIs as a reduction in replication rate
462 results in exponential differences with time. This suggest that polymerase activity of NL09
463 is higher than NL11 and that the faster kinetics in virus replication observed in NL11
464 infected cells may be due to more efficient virus entry, release, or immune evasion than
465 NL09.

466 In addition to its role in viral entry, we previously demonstrated that FAK regulates the
467 polymerase activity *in vitro* of multiple IAV strains using Y15 as well as dominant-negative
468 kinase mutants ²⁹. However, in contrast to our previous studies, we only observed a
469 modest and non-significant effect on polymerase activity following DF treatment. O'Brien
470 et al. showed that Y15 was a significantly more potent and selective inhibitor of FAK
471 activity than DF which also targets the FAK related kinase Pyk2 ⁸³. The disparity between
472 a given SMKI's binding affinity (K_d) and its functional inhibitory concentrations can also
473 be observed in the case of a single inhibitor targeting multiple kinases. For instance, the
474 K_d of the multi-kinase inhibitor Sunitinib for TrkC is 5.1 μM , but a 10-fold lower
475 concentration (0.5 μM) is sufficient to inhibit >97% of its activity. In contrast, Sunitinib's
476 K_d for PAK3 is 16 nM, but not even a 30-fold higher concentration (0.48 μM) has an effect
477 on its activity ⁶⁷. Therefore, the difference in potency of FAK inhibition by DF vs Y15 may
478 account for the limited effect of DF treatment on IAV polymerase activity we observed.

479 Inhibition of Src by SA, BTK and EGFR by IB, and BTK by AC had less of a significant
480 effect on IAV polymerase activity indicating that the contribution of these kinases to host
481 innate immune responses does not directly affect RNA replication. In contrast, inhibition

482 of Abl and PDGFR α by NI treatment had the most significant reduction in IAV polymerase
483 activity that was also strain independent. These data point to a role of PDGFR α in
484 facilitating efficient IAV polymerase activity. This is consistent with previous findings that
485 show inhibition of PDGFR α by the RTK inhibitor A9, blocks RNA synthesis of all viral RNA
486 species (vRNA, cRNA and mRNA) independently of NF κ B signaling⁵⁶.

487 The NF κ B pathway typically mediates inflammatory/antiviral responses to viral
488 infections and accordingly, it plays a critical role in IAV replication and pathogenesis.
489 Several reports indicate that IAVs modulate antiviral NF κ B activity to facilitate viral
490 replication. Inhibition of NF κ B results in reduced viral titers partly due to a disruption of
491 vRNP nuclear export⁸⁴⁻⁸⁶. Consistent with previous data, we did not observe a robust
492 induction in NF κ B phosphorylation, most likely due to the immuno-suppressive role of the
493 viral NS1 protein⁸⁷. However, we observed a clear induction of NF κ B activation by
494 poly(IC) treatment alone or in combination with IAV infection at 18 h but not 48 h.

495 In addition to its role in actin reorganization, FAK modulates the cellular immune
496 response by regulating various T-cell-, B-cell-, and macrophage-functions as well as RIG-
497 I-Like antiviral signaling⁸⁸⁻⁹¹. We previously demonstrated FAK-dependent regulation of
498 NF κ B signaling and polymerase activity *in vitro* and NF κ B-dependent pro-inflammatory
499 responses *in vivo*³⁰. In that study, FAK inhibition resulted in increased survival, reduced
500 viral load and reduction in a severe infection model. Surprisingly, DF treatment had no
501 significant effect on NF κ B phosphorylation; this again, is likely due to the difference in
502 FAK inhibition potency between Y15 and DF. Similarly, none of the other NRTKs
503 influenced NF κ B activation suggesting that the mechanism by which these NRTKs inhibit
504 virus replication is independent of the NF κ B-pathway. Considering the transient and

505 biphasic nature of NFkB activation, we cannot rule out that strain-dependent differences
506 in kinetics did not affect the magnitude or duration of NFkB activation we observed^{92,93}.

507 An emerging regulator of IFN and inflammatory responses is STAT3. A wide range of
508 cytokine, growth factor, and RTKs activate STAT3 via JAK1/2/3 and Tyk2-dependent
509 phosphorylation at Y705 (STAT3pY705)⁹⁴. The role of STAT3 is not fully understood with
510 opposing functions dependent on pathway partner; IL-6 mediated STAT3 activation is
511 proinflammatory while IL-10 mediated STAT3 activation is anti-inflammatory^{94,95}.
512 Although STAT3 is dispensable for IFN signaling, it is activated by IFN-I and serves as a
513 negative regulator to fine-tune the IFN response (reviewed in⁹⁵). Because STAT3
514 activation upregulates anti-apoptotic factors, H5N1 mediated STAT3pY705 allows
515 prolonged viral production through delay of apoptosis; H1N1 is less efficient at
516 STAT3pY705 and triggers apoptosis earlier^{96,97}. Although the mechanism of differential
517 suppression of STAT3 activation by IAV is not clear, it has been suggested to be mediated
518 by NS1⁸⁷. Interestingly, EGFR activation can result in Src/FAK/BTK mediated activation
519 of STAT3, thereby modulating the IFN and proinflammatory responses. As expected of
520 H1N1 and H3N2 infections^{96,97}, we observed a suppression of STAT3pY705 in untreated
521 cells that was comparable to that observed following treatment with most NRTKIs.
522 Surprisingly, we observed significant suppression of STATpY705 following DF treatment
523 (85-90% of untreated infected cells). Considering that DF inhibits both FAK and Pyk2, it
524 is tempting to speculate that STAT3pY705 requires FAK/Pyk2 activity during IAV
525 infection. Indeed, Pyk2 kinase activity was required to induce EGFR/Src-mediated
526 STAT3pY705⁹⁸. Interestingly, STAT3pS727 which is required for full transcriptional

527 activity of STAT3, points to an indirect Pyk2 mechanism possibly through JNK, p38 or
528 ERK activation ⁹⁸.

529 In summary, we have demonstrated that NRTKs are host cell factors required for
530 efficient IAV replication and represent promising drug targets for the development of the
531 next generation of antivirals. Because these inhibitors target host factors, their therapeutic
532 window is likely to be different than that of virus-targeted antivirals. To our surprise, our
533 tested NRTKIs directly affected steps of the virus replication cycle with limited effects on
534 tested host responses. Importantly, our results were validated using an *ex vivo* lung tissue
535 model from several donors. Given that most of our PCLS were obtained from lung cancer
536 tumor resections, our donors tend to be older, are often smokers and suffer from either
537 COPD or other respiratory pathologies. Although at first glance this may seem like a
538 limitation of our model, we believe that these donors represent the “at risk” populations
539 that would most benefit from IAV antivirals. Therefore, our data obtained from donor
540 PCLS using these already FDA-approved NRTKIs as IAV antivirals is highly applicable to
541 clinical settings. In contrast to virus-directed IAV antivirals which are susceptible to
542 resistance mutations, our data indicate a high genetic barrier for resistance to our tested
543 NRTKIs. This is based on the stability of IAV inhibition after 5 passages under selective
544 pressure by each of our six validated inhibitors. Although we cannot rule out NRTKIs-
545 selected mutations, no resistance/adaptive variants were detected. Additionally, their
546 established safety and bioavailability data further warrants the evaluation of these
547 compounds as potential influenza treatments. Given that IAV infections are typically
548 restricted to the respiratory tract, localized delivery of the kinase inhibitors can further limit
549 potential cytotoxic effects. Finally, the local microenvironment must be considered to elicit

550 a balanced immune response. Likewise, the effect of promising kinase inhibitors on
551 resident and infiltrating immune cells must be investigated to avoid opposite or
552 unintended consequences. Considering that many viruses, including respiratory viruses,
553 utilize the same (or related) host kinases to facilitate their replication and transmission,
554 our studies have broader implications for the potential use of these SMKIs to treat
555 infections by other viruses in addition to IAV infections.

556 **MATERIALS AND METHODS**

557 ***Cells and Viruses.*** Madin-Darby canine kidney (MDCK) cells were cultured in Dulbecco's
558 modified Eagle medium (DMEM; Gibco) supplemented with 10% fetal bovine serum
559 (FBS), 100 IU/mL penicillin, 100 µg/mL streptomycin, 2 mM glutamine, and 1%
560 nonessential amino acids (NEAAs). A549 cells were cultured in F-12 K-Nut Nutrient Mix
561 medium (Gibco) supplemented with 10% FBS, 100 IU/ml penicillin, 100 µg/ml
562 streptomycin, and 2 mM Glutamax. All cells were incubated at 37°C and 5% CO₂.

563 The pandemic H1N1 strain A/Netherlands/602/09 (NL09) and seasonal strain H3N2
564 A/Netherlands/241/11 (NL11) influenza viruses were obtained from the Repository of the
565 National Influenza Center at the Erasmus Medical Center in Rotterdam, the Netherlands,
566 and were grown on MDCKs for 48h at 37 °C. Virus stocks and culture supernatants were
567 stored at -80°C until further use. Virus yields were titrated on MDCK cells by 50% tissue
568 culture infectious dose (TCID₅₀)/ml method as described by Reed and Muensch⁹⁹.

569
570 ***Human precision-cut lung slices (PCLS).*** Human PCLS for *ex vivo* studies were
571 generated from lung tissues obtained from patients undergoing surgical operations at
572 Hannover Medical School. Tissues used for PCLS generation that were obtained from
573 lung tumor resections were confirmed as tumor-free by an experienced pathologist. The
574 freshly obtained lung tissues were processed into circular slices that were 300 microns
575 thick and 8 mm in diameter as previously described³⁴. All donors provided informed
576 consent as approved by the Hannover Medical School Ethics Committee (Ethics vote
577 #8867_BO_K_2020). PCLS were maintained in DMEM/F12 medium (ThermoFisher)

578 supplemented with 2 mM of HEPES, 1 × GlutaMAX (Gibco), 100 U/ml penicillin and 100
579 µg/ml streptomycin in a humidified 37°C and 5% CO₂ incubator.

580

581 ***Inhibitors.*** Small molecule kinase inhibitors (SMKI) were all purchased from Selleckchem
582 (TX, USA). Inhibitors were diluted in DMSO to a stock concentration of 10mM and stored
583 at -20°C upon usage.

584

585 ***In vitro and ex vivo cytotoxicity assays.*** *In vitro* cytotoxicity of SMKIs on mock and/or
586 virus infected A549 cells was determined using CellTiter-Glo 2.0 (CTG) Cell Viability
587 Assay (Promega) according to manufacturer protocols.

588 Cytotoxicity of SMKIs on mock and/or virus-infected PCLS was determined using the
589 LDH-Glo Cytotoxicity Assay (Promega) according to manufacturer's protocols.
590 Supernatants of SMKI-treated and untreated hPCLS were collected and completely
591 replaced with fresh pre-warmed infection medium containing SMKIs at the indicated
592 concentrations. LDH levels were relative to the positive control (treated with 1% triton-X
593 100 for 30 min at 37°C).

594

595 ***Virus infections.*** A549 cells were plated on the day prior to infection so they were 80-
596 90% confluent on the day of infection. For infections, viruses were diluted in infection
597 medium (F12K containing 0.1% [vol/vol] bovine serum albumin [BSA] and 50 ng/µl TPCK-
598 treated trypsin). The cells were inoculated with the virus at the indicated multiplicity of
599 infection (MOI) for 1h at 37°C. The cells were washed twice with phosphate-buffered
600 saline containing Mg²⁺/Ca²⁺ (PBS+/+) to remove unbound virus and incubated in infection

601 medium at 37°C in the presence or absence of SMKIs at the indicated concentrations.
602 Supernatants were collected at 0, 24, 48, 72 hours post-infection (hpi), and viral titers
603 were determined by TCID₅₀ assay in MDCK cells⁹⁹. GraphPad's Heatmap (Prism)
604 function was used to visualize the fold-reduction in viral titers.

605

606 ***Immunofluorescent staining and imaging.*** To visualize virus infection, infected cells
607 were fixed with 4% paraformaldehyde (4% PFA) for 30 minutes at room temperature (RT),
608 permeabilized with 0.1% Triton X-100 for 15 minutes at RT, washed with PBS and blocked
609 with heat inactivated 5% horse serum in PBS (PBS-HS) at RT for 1h. Cells were then
610 incubated with mouse monoclonal antibodies to IAV nucleoprotein (clone HB65, ATCC)
611 diluted in PBS-HS at 0.2 µg/ml overnight at 4°C under constant agitation. Cells were
612 washed and incubated with AlexaFluor-594 conjugated goat anti-mouse IgG antibody (0.2
613 µg/ml; ThermoFisher) and NucBlue Live ReadyProbes Reagent (ThermoFisher) for 1h at
614 RT under constant agitation. Cells were washed 3 times with PBS, images were captured
615 using a Leica DMI8 fluorescence microscope and quantitative analysis was performed
616 using ImageJ Threshold, Watershed, and Particle Analyser tools.

617 Using a counting macro that we adapted from¹⁰⁰, we quantified the number of nuclei
618 and the number of separate infected cells by analyzing the RAW image data for each
619 channel (n=4). The nucleus count was used to define the total cell number per 0.6 mm².
620 The NP staining was used to define the number of infected cells per 0.6 mm². The ratio
621 of infected to total cells was used to calculate Relative Infectivity. The total number of
622 cells based on nuclei detected relative to mock-infected cells treated with the respective

623 NRTKI was used to determine Relative Viability. GraphPad's Heatmap (Prism) function
624 was used for visualization.

625

626 ***Immuno-histochemistry staining.*** Mock- and virus-Infected PCLS were inactivated by
627 fixation in 4% PFA/PBS and paraffin-embedded into blocks. Tissue sections (2 μ m thick)
628 were cut from the paraffin-embedded blocks and subjected to Hematoxylin & Eosin (HE)
629 staining using standard protocols. Immunostaining for IAV antigen was done using a
630 HRP-conjugated anti-IAV NP antibody. Histological analysis was performed by an
631 experienced pathologist blinded to clinical data and experimental setup using a routine
632 diagnostic light microscope (BX43, Olympus). Representative images were acquired with
633 an Olympus CS50 camera using Olympus CellSens software (Olympus). Semi-
634 quantitative analysis of IAV NP signal was performed for all tested NRTKIs using FIJI
635 image-analysis software.

636

637 ***Polymerase activity assay.*** Semi-confluent (~70–80%) A549 cells (8×10^4 cells in 24-
638 well plates) were transfected using Lipofectamine LTX with The pPOLI-358-FFLuc
639 reporter plasmid, which encodes a firefly luciferase gene under control of the viral
640 nucleoprotein (NP) promoter (kindly provided by Megan Shaw)⁵⁰⁻⁵²; the Lonza
641 pmaxGFP™ expression vector, was used as a transfection control.

642 For minigenome polymerase activity, a mix of plasmids encoding the PB2, PB1, PA, and
643 NP genes of NL09 or A/NL/213/03 (H3N2) IAVs in quantities of 0.35, 0.35, 0.35, and 0.5
644 μ g, respectively, were co-transfected with the reporter and control plasmids. At 6h post-
645 transfection (hpt), the indicated SMKIs were added at 1x and 0.5x concentrations (see

646 Table 1) and at 30 hpt (24h of treatment), luciferase reporter activity was detected using
647 the One-Glo luciferase assay system (Promega). GFP mean fluorescence intensity (MFI)
648 and luciferase luminescence were measured using a Tecan multi-mode plate reader.

649 To measure polymerase activity during IAV infection, cells were infected at an MOI of
650 1 with NL09 or NL11 at 24h post-transfection (hpt) of the pPOLI-358-FFLuc reporter and
651 the GFP plasmids in the presence or absence of SMKIs at the indicated concentrations
652 as described above. At 48 hpt (24 hpi), luciferase reporter activity was detected using the
653 One-Glo luciferase assay system (Promega). GFP mean fluorescence intensity (MFI) and
654 luciferase luminescence were measured using a Tecan multi-mode plate reader.

655

656 ***Viral entry assay and confocal microscopy.*** A549 cells were seeded on 12.5-mm
657 coverslips in 24-well plates. On the day of infection, cells were washed 3 times with
658 PBS+/+ and incubated in infection medium in the presence or absence of kinase inhibitors
659 for 2h. The cells were chilled on ice for 15 min and inoculated with virus (MOI=10) in the
660 presence or absence of the indicated SMKI concentrations at 4°C and on ice for 30 min.
661 To limit receptor activation due to continuous viral-receptor engagement/internalization
662 following the 4°C adsorption and to gently warm up the cells, unbound/noninternalized
663 virus was removed by washing the cells twice with RT PBS+/+. The cells were then
664 incubated with prewarmed infection medium containing the respective SMKIs at 37°C for
665 30 min. Cells were then fixed in 4% PFA for 30 min, permeabilized with 0.1% Triton X-
666 100 at RT for 15 min, washed in PBS, and incubated overnight at 4°C in blocking buffer
667 (PBS-HS). The cells were then incubated with anti-IAV NP antibody (clone HB65, ATCC)
668 diluted in blocking buffer for 1h at RT, washed 3 times with PBS, and incubated for 1h at

669 RT with AlexaFluor488-conjugated donkey anti-mouse IgG secondary antibody (0.2
670 $\mu\text{g/ml}$; ThermoFisher) diluted PBS-HS. Cell nuclei and F-Actin were stained with NucBlue
671 Live ReadyProbes (ThermoFisher) and ActinRed-555 ReadyProbes Reagent
672 (ThermoFisher), respectively. Coverslips were mounted with Prolong mounting medium
673 (Invitrogen), and cell images were acquired with a Leica TSC SP5 laser-scanning
674 confocal system mounted on an upright Leica DM6000 CFS using a 63x oil immersion
675 objective. The images were merged and analyzed with Leica LAS software using identical
676 imaging settings across all experiments.

677

678 ***NRTKI resistance analysis.*** To assess the resistance barrier for our NRTKIs, we
679 passaged our viruses five times in the presence or absence of submaximal inhibitor
680 concentrations (0.5x; see table 1). The parental viruses were also passaged under the
681 same culture conditions in parallel in the absence of NRTKIs. Semi-confluent MDCK cells
682 ($\sim 10^6$ cells/well in 6-well plates) were infected with the pandemic H1N1 strain
683 A/Netherlands/602/09 (NL09) and seasonal strain H3N2 A/Netherlands/241/11 (NL11) at
684 MOI 0.001. At each passage, the cultures were maintained in 3 ml MDCK infection media
685 at 37°C for 72h, in the presence or absence of the $[0.5x]_{\text{max}}$ (see Tab. 1) of respective
686 candidate NRTKIs. Supernatants were harvested, clarified by centrifugation at 500 x g for
687 5 min at 4°C, and stored at -80°C until titration by TCID₅₀ assay on MDCK cells. For the
688 subsequent passage, cells were infected by using virus from the previous passage at
689 MOI=0.001.

690

691 **SDS-PAGE and immunoblotting.** Proteins were isolated from whole cell lysates using
692 the M-PER Mammalian Protein Extraction Reagent (ThermoScientific). Proteins were
693 quantified by Bradford Assay, separated by 8% SDS-PAGE, transferred onto a PVDF
694 membrane and blocked overnight in blocking solution (TBS pH7.6, 0.05% Tween-20, and
695 5% w/v of nonfat dry milk). Primary antibodies were diluted in blocking solution overnight
696 at 4°C: phos-NFkB p65 (Ser536) (93H1) Rabbit mAb (1:1000) (Cell Signaling), phos-Stat3
697 (Tyr705) (D3A7) rabbit mAb (1:1000) (Cell Signaling), Influenza A virus NP Antibody
698 (PA5-32242) rabbit pAb (1:20,000) (ThermoScientific). Beta-Actin (BA3R) mAb (1:5000)
699 was used as a loading control. HRP-conjugated secondary anti-rabbit or anti-mouse
700 antibodies (1:20,000) were diluted in blocking solution for 1 hour at room temperature.
701 Proteins were detected by chemiluminescence using the SuperSignal West Pico Plus and
702 SuperSignal™ West Femto Maximum Sensitivity Substrate. Band density was measured
703 using a Li-Cor C-DiGit scanner and analyzed using Image Studio™ (Li-Cor). When
704 necessary, the imaged membrane was subsequently stripped using a mild water-based
705 stripping solution (1.5% glycine; 0.1% SDS; 1% Tween-20; pH 2.2) and restained for total
706 proteins using NFkB p65 (L8F6) mouse mAb (1:1000) (Cell Signaling) or Stat3 (124H6)
707 mouse mAb (1:1000) (Cell Signaling).

708

709 **Statistical analyses.** Statistical analyses with GraphPad Prism 9 included multiple *t* test,
710 Brown-Forsythe and Welch's ANOVA tests and Dunnett's T3 test for multiple
711 comparisons. Values are represented as means standard deviations (SD) or standard
712 error of the mean (SEM), with a *P* value of 0.05 considered statistically significant (ns =

713 $P > 0.05$; * = $P \leq 0.05$; ** = $P \leq 0.01$; *** = $P \leq 0.001$; **** = $P \leq 0.0001$). The performed
714 tests and given significances are provided in the figure legends.

715

716

717

718

719 **ACKNOWLEDGMENTS**

720 This work was supported by the Alexander von Humboldt Foundation in the framework
721 of the Alexander von Humboldt Professorship endowed by the German Federal Ministry
722 of Education and Research; and by the European Union's Horizon 2020 Research and
723 Innovation Program grant number 848166 [ISOLDA]. DJ is supported by a European
724 Consolidator grant, XHale (ref. no. 771883). The author's would like to thank Regina
725 Engelhardt, Nicole Kröncke, Annette Müller-Brechlin and Christina Petzold-Mügge for
726 their extraordinary technical support.

727

728 **AUTHOR CONTRIBUTIONS**

729 HE conceived the project. HE, RM and GR designed the experiments and supervised the
730 project. RM, SS, MB performed the experiments. HE, RM, conducted data analysis. CW,
731 MK and DJ generated and provided human PCLS. CW and MK provided histopathological
732 and immunohistochemical evaluation of PCLS. RM, GR and HE wrote the manuscript
733 with input from all the authors.

734

735 **CONFLICT OF INTEREST**

736 The authors declare no conflict of interest.

REFERENCES

- 737
738
- 739 1 Elbahesh, H., Saletti, G., Gerlach, T. & Rimmelzwaan, G. F. Broadly protective
740 influenza vaccines: design and production platforms. *Curr Opin Virol* **34**, 1-9,
741 doi:10.1016/j.coviro.2018.11.005 (2019).
- 742 2 Jansen, J. M., Gerlach, T., Elbahesh, H., Rimmelzwaan, G. F. & Saletti, G. Influenza
743 virus-specific CD4+ and CD8+ T cell-mediated immunity induced by infection and
744 vaccination. *J Clin Virol* **119**, 44-52, doi:10.1016/j.jcv.2019.08.009 (2019).
- 745 3 Wong, S.-S. & Webby, R. J. Traditional and new influenza vaccines. *Clinical*
746 *microbiology reviews* **26**, 476-492, doi:10.1128/CMR.00097-12 (2013).
- 747 4 Webster, R. G. & Govorkova, E. A. Continuing challenges in influenza. *Annals of the*
748 *New York Academy of Sciences* **1323**, 115-139, doi:10.1111/nyas.12462 (2014).
- 749 5 Nelson, M. I., Simonsen, L., Viboud, C., Miller, M. A. & Holmes, E. C. The origin and
750 global emergence of adamantane resistant A/H3N2 influenza viruses. *Virology* **388**,
751 270-278, doi:10.1016/j.virol.2009.03.026 (2009).
- 752 6 Lackenby, A. *et al.* Global update on the susceptibility of human influenza viruses to
753 neuraminidase inhibitors and status of novel antivirals, 2016-2017. *Antiviral research*
754 **157**, 38-46, doi:10.1016/j.antiviral.2018.07.001 (2018).
- 755 7 Baranovich, T. *et al.* The neuraminidase inhibitor oseltamivir is effective against
756 A/Anhui/1/2013 (H7N9) influenza virus in a mouse model of acute respiratory
757 distress syndrome. *The Journal of infectious diseases* **209**, 1343-1353,
758 doi:10.1093/infdis/jit554 (2014).

- 759 8 Mifsud, E. J., Hayden, F. G. & Hurt, A. C. Antivirals targeting the polymerase
760 complex of influenza viruses. *Antiviral research* **169**, 104545,
761 doi:10.1016/j.antiviral.2019.104545 (2019).
- 762 9 Mullard, A. FDA approves first new flu drug in 20 years. *Nat Rev Drug Discov* **17**,
763 853, doi:10.1038/nrd.2018.219 (2018).
- 764 10 Hayden, F. G. *et al.* Baloxavir Marboxil for Uncomplicated Influenza in Adults and
765 Adolescents. *N Engl J Med* **379**, 913-923, doi:10.1056/NEJMoa1716197 (2018).
- 766 11 Omoto, S. *et al.* Characterization of influenza virus variants induced by treatment
767 with the endonuclease inhibitor baloxavir marboxil. *Sci Rep* **8**, 9633,
768 doi:10.1038/s41598-018-27890-4 (2018).
- 769 12 Uehara, T. *et al.* Treatment-Emergent Influenza Variant Viruses With Reduced
770 Baloxavir Susceptibility: Impact on Clinical and Virologic Outcomes in
771 Uncomplicated Influenza. *The Journal of infectious diseases* **221**, 346-355,
772 doi:10.1093/infdis/jiz244 (2020).
- 773 13 Meineke, R., Rimmelzwaan, G. F. & Elbahesh, H. Influenza Virus Infections and
774 Cellular Kinases. *Viruses* **11**, doi:10.3390/v11020171 (2019).
- 775 14 Kumar, N. *et al.* Host-Directed Antiviral Therapy. *Clin Microbiol Rev* **33**,
776 doi:10.1128/CMR.00168-19 (2020).
- 777 15 Watanabe, T., Watanabe, S. & Kawaoka, Y. Cellular networks involved in the
778 influenza virus life cycle. *Cell Host Microbe* **7**, 427-439,
779 doi:10.1016/j.chom.2010.05.008 (2010).

- 780 16 Schwartz, D. M. *et al.* JAK inhibition as a therapeutic strategy for immune and
781 inflammatory diseases. *Nature reviews. Drug discovery* **17**, 78-78,
782 doi:10.1038/nrd.2017.267 (2017).
- 783 17 Ludwig, S., Zell, R., Schwemmler, M. & Herold, S. Influenza, a One Health paradigm-
784 -novel therapeutic strategies to fight a zoonotic pathogen with pandemic potential.
785 *Int J Med Microbiol* **304**, 894-901, doi:10.1016/j.ijmm.2014.08.016 (2014).
- 786 18 Kumar, N., Sharma, N. R., Ly, H., Parslow, T. G. & Liang, Y. Receptor tyrosine
787 kinase inhibitors that block replication of influenza a and other viruses. *Antimicrobial*
788 *agents and chemotherapy* **55**, 5553-5559, doi:10.1128/AAC.00725-11 (2011).
- 789 19 Johnson, L. N. & Lewis, R. J. Structural basis for control by phosphorylation. *Chem*
790 *Rev* **101**, 2209-2242 (2001).
- 791 20 Manning, G., Whyte, D. B., Martinez, R., Hunter, T. & Sudarsanam, S. The protein
792 kinase complement of the human genome. *Science (New York, N.Y.)* **298**, 1912-
793 1934, doi:10.1126/science.1075762 (2002).
- 794 21 Turner, N. & Grose, R. Fibroblast growth factor signalling: from development to
795 cancer. *Nat Rev Cancer* **10**, 116-129, doi:10.1038/nrc2780 (2010).
- 796 22 Frojdo, S., Vidal, H. & Pirola, L. Alterations of insulin signaling in type 2 diabetes: a
797 review of the current evidence from humans. *Biochim Biophys Acta* **1792**, 83-92,
798 doi:10.1016/j.bbadis.2008.10.019 (2009).
- 799 23 Flight, M. H. Neurodegenerative diseases: New kinase targets for Alzheimer's
800 disease. *Nat Rev Drug Discov* **12**, 739, doi:10.1038/nrd4132 (2013).

- 801 24 Siveen, K. S. *et al.* Role of Non Receptor Tyrosine Kinases in Hematological
802 Malignances and its Targeting by Natural Products. *Mol Cancer* **17**, 31,
803 doi:10.1186/s12943-018-0788-y (2018).
- 804 25 Azevedo, A., Silva, S. & Rueff, J. Non-receptor Tyrosine Kinases Role and
805 Significance in Hematological Malignancies. *Tyrosine Kinases as Druggable Targets*
806 *in Cancer*, doi:10.5772/intechopen.84873 (2019).
- 807 26 Roskoski, R., Jr. Properties of FDA-approved small molecule protein kinase
808 inhibitors: A 2021 update. *Pharmacol Res* **165**, 105463,
809 doi:10.1016/j.phrs.2021.105463 (2021).
- 810 27 Florence, J. M. *et al.* Inhibiting Bruton's tyrosine kinase rescues mice from lethal
811 influenza-induced acute lung injury. *American journal of physiology. Lung cellular*
812 *and molecular physiology* **315**, L52-L58, doi:10.1152/ajplung.00047.2018 (2018).
- 813 28 Elbahesh, H. *et al.* Novel roles of focal adhesion kinase in cytoplasmic entry and
814 replication of influenza A viruses. *Journal of virology* **88**, 6714-6728,
815 doi:10.1128/JVI.00530-14 (2014).
- 816 29 Elbahesh, H., Bergmann, S. & Russell, C. J. Focal adhesion kinase (FAK) regulates
817 polymerase activity of multiple influenza A virus subtypes. *Virology* **499**, 369-374,
818 doi:10.1016/j.virol.2016.10.002 (2016).
- 819 30 Bergmann, S. & Elbahesh, H. Targeting the proviral host kinase, FAK, limits
820 influenza a virus pathogenesis and NFkB-regulated pro-inflammatory responses.
821 *Virology* **534**, 54-63, doi:10.1016/j.virol.2019.05.020 (2019).

- 822 31 Ghoreschi, K. *et al.* Modulation of Innate and Adaptive Immune Responses by
823 Tofacitinib (CP-690,550). *The Journal of Immunology* **186**, 4234-4243,
824 doi:10.4049/jimmunol.1003668 (2011).
- 825 32 Boor, P. P. C. *et al.* JAK-inhibitor tofacitinib suppresses interferon alfa production by
826 plasmacytoid dendritic cells and inhibits arthrogenic and antiviral effects of interferon
827 alfa. *Translational Research* **188**, 67-79,
828 doi:<https://doi.org/10.1016/j.trsl.2016.11.006> (2017).
- 829 33 Liu, G. *et al.* Use of precision cut lung slices as a translational model for the study of
830 lung biology. *Respir Res* **20**, 162, doi:10.1186/s12931-019-1131-x (2019).
- 831 34 Preuss, E. B. *et al.* The Challenge of Long-Term Cultivation of Human Precision-Cut
832 Lung Slices. *Am J Pathol*, doi:10.1016/j.ajpath.2021.10.020 (2021).
- 833 35 Viana, F., O'Kane, C. M. & Schroeder, G. N. Precision-cut lung slices: A powerful ex
834 vivo model to investigate respiratory infectious diseases. *Mol Microbiol*,
835 doi:10.1111/mmi.14817 (2021).
- 836 36 Changelian, P. S. *et al.* Prevention of organ allograft rejection by a specific Janus
837 kinase 3 inhibitor. *Science (New York, N.Y.)* **302**, 875-878,
838 doi:10.1126/science.1087061 (2003).
- 839 37 Quintás-Cardama, A. *et al.* Preclinical characterization of the selective JAK1/2
840 inhibitor INCB018424: therapeutic implications for the treatment of myeloproliferative
841 neoplasms. *Blood* **115**, 3109-3117, doi:10.1182/blood-2009-04-214957 (2010).
- 842 38 Manley, P. W. *et al.* Extended kinase profile and properties of the protein kinase
843 inhibitor nilotinib. *Biochimica et biophysica acta* **1804**, 445-453,
844 doi:10.1016/j.bbapap.2009.11.008 (2010).

- 845 39 Weisberg, E. *et al.* Beneficial effects of combining nilotinib and imatinib in preclinical
846 models of BCR-ABL+ leukemias. *Blood* **109**, 2112-2120, doi:10.1182/blood-2006-
847 06-026377 (2007).
- 848 40 Boschelli, D. H. *et al.* Optimization of 4-phenylamino-3-quinolinecarbonitriles as
849 potent inhibitors of Src kinase activity. *J Med Chem* **44**, 3965-3977,
850 doi:10.1021/jm0102250 (2001).
- 851 41 Golas, J. M. *et al.* SKI-606, a 4-anilino-3-quinolinecarbonitrile dual inhibitor of Src
852 and Abl kinases, is a potent antiproliferative agent against chronic myelogenous
853 leukemia cells in culture and causes regression of K562 xenografts in nude mice.
854 *Cancer Res* **63**, 375-381 (2003).
- 855 42 Roskoski, R., Jr. Src protein-tyrosine kinase structure, mechanism, and small
856 molecule inhibitors. *Pharmacol Res* **94**, 9-25, doi:10.1016/j.phrs.2015.01.003 (2015).
- 857 43 Covey, T. *et al.* ACP-196: a novel covalent Bruton's tyrosine kinase (Btk) inhibitor
858 with improved selectivity and in vivo target coverage in chronic lymphocytic leukemia
859 (CLL) patients. *Cancer Research* **75**, 2596-2596, doi:10.1158/1538-7445.Am2015-
860 2596 (2015).
- 861 44 Wu, J., Zhang, M. & Liu, D. Acabrutinib (ACP-196): a selective second-generation
862 BTK inhibitor. *J Hematol Oncol* **9**, 21, doi:10.1186/s13045-016-0250-9 (2016).
- 863 45 Honigberg, L. A. *et al.* The Bruton tyrosine kinase inhibitor PCI-32765 blocks B-cell
864 activation and is efficacious in models of autoimmune disease and B-cell
865 malignancy. *Proc Natl Acad Sci U S A* **107**, 13075-13080,
866 doi:10.1073/pnas.1004594107 (2010).

- 867 46 Gao, W. *et al.* Selective antitumor activity of ibrutinib in EGFR-mutant non-small cell
868 lung cancer cells. *J Natl Cancer Inst* **106**, doi:10.1093/jnci/dju204 (2014).
- 869 47 Kang, Y. *et al.* Role of focal adhesion kinase in regulating YB-1-mediated paclitaxel
870 resistance in ovarian cancer. *J Natl Cancer Inst* **105**, 1485-1495,
871 doi:10.1093/jnci/djt210 (2013).
- 872 48 Boivin, S., Cusack, S., Ruigrok, R. W. & Hart, D. J. Influenza A virus polymerase:
873 structural insights into replication and host adaptation mechanisms. *The Journal of*
874 *biological chemistry* **285**, 28411-28417, doi:10.1074/jbc.R110.117531 (2010).
- 875 49 Baranovich, T. *et al.* T-705 (favipiravir) induces lethal mutagenesis in influenza A
876 H1N1 viruses in vitro. *Journal of virology* **87**, 3741-3751, doi:10.1128/JVI.02346-12
877 (2013).
- 878 50 Azzeh, M., Flick, R. & Hobom, G. Functional analysis of the influenza A virus cRNA
879 promoter and construction of an ambisense transcription system. *Virology* **289**, 400-
880 410, doi:10.1006/viro.2001.1107 (2001).
- 881 51 Deng, T., Sharps, J. L. & Brownlee, G. G. Role of the influenza virus heterotrimeric
882 RNA polymerase complex in the initiation of replication. *The Journal of general*
883 *virology* **87**, 3373-3377, doi:10.1099/vir.0.82199-0 (2006).
- 884 52 Hoffmann, H. H., Palese, P. & Shaw, M. L. Modulation of influenza virus replication
885 by alteration of sodium ion transport and protein kinase C activity. *Antiviral research*
886 **80**, 124-134, doi:10.1016/j.antiviral.2008.05.008 (2008).
- 887 53 Roux, P. P. & Blenis, J. ERK and p38 MAPK-Activated Protein Kinases: a Family of
888 Protein Kinases with Diverse Biological Functions. **68**, 320-344,

- 889 doi:10.1128/MMBR.68.2.320-344.2004 %J Microbiology and Molecular Biology
890 Reviews (2004).
- 891 54 Arrese, M. & Portela, A. Serine 3 is critical for phosphorylation at the N-terminal end
892 of the nucleoprotein of influenza virus A/Victoria/3/75. *Journal of virology* **70**, 3385-
893 3391 (1996).
- 894 55 Hsiang, T. Y., Zhou, L. & Krug, R. M. Roles of the phosphorylation of specific serines
895 and threonines in the NS1 protein of human influenza A viruses. *J Virol* **86**, 10370-
896 10376, doi:10.1128/JVI.00732-12 (2012).
- 897 56 Kumar, N., Liang, Y., Parslow, T. G. & Liang, Y. Receptor tyrosine kinase inhibitors
898 block multiple steps of influenza a virus replication. *J Virol* **85**, 2818-2827,
899 doi:10.1128/jvi.01969-10 (2011).
- 900 57 Kurokawa, M., Ochiai, H., Nakajima, K. & Niwayama, S. Inhibitory effect of protein
901 kinase C inhibitor on the replication of influenza type A virus. *J Gen Virol* **71 (Pt 9)**,
902 2149-2155, doi:10.1099/0022-1317-71-9-2149 (1990).
- 903 58 Ludwig, S. Targeting cell signalling pathways to fight the flu: towards a paradigm
904 change in anti-influenza therapy. *The Journal of antimicrobial chemotherapy* **64**, 1-4,
905 doi:10.1093/jac/dkp161 (2009).
- 906 59 Marjuki, H. *et al.* Influenza A virus-induced early activation of ERK and PI3K
907 mediates V-ATPase-dependent intracellular pH change required for fusion. *Cellular*
908 *microbiology* **13**, 587-601, doi:10.1111/j.1462-5822.2010.01556.x (2011).
- 909 60 Planz, O. Development of cellular signaling pathway inhibitors as new antivirals
910 against influenza. *Antiviral research* **98**, 457-468, doi:10.1016/j.antiviral.2013.04.008
911 (2013).

- 912 61 Wang, S. *et al.* Tyrosine 132 phosphorylation of influenza A virus M1 protein is
913 crucial for virus replication by controlling the nuclear import of M1. *Journal of virology*
914 **87**, 6182-6191, doi:10.1128/JVI.03024-12 (2013).
- 915 62 Xie, J. *et al.* Regulatory roles of c-jun in H5N1 influenza virus replication and host
916 inflammation. *Biochimica et biophysica acta* **1842**, 2479-2488,
917 doi:10.1016/j.bbadis.2014.04.017 (2014).
- 918 63 Turrell, L., Hutchinson, E. C., Vreede, F. T. & Fodor, E. Regulation of influenza A
919 virus nucleoprotein oligomerization by phosphorylation. *J Virol* **89**, 1452-1455,
920 doi:10.1128/JVI.02332-14 (2015).
- 921 64 York, A., Hutchinson, E. C. & Fodor, E. Interactome analysis of the influenza A virus
922 transcription/replication machinery identifies protein phosphatase 6 as a cellular
923 factor required for efficient virus replication. *J Virol* **88**, 13284-13299,
924 doi:10.1128/JVI.01813-14 (2014).
- 925 65 Hutchinson, E. C. *et al.* Mapping the phosphoproteome of influenza A and B viruses
926 by mass spectrometry. *PLoS Pathog* **8**, e1002993,
927 doi:10.1371/journal.ppat.1002993 (2012).
- 928 66 Kirchhoff, J. *et al.* Infection of differentiated airway epithelial cells from caprine lungs
929 by viruses of the bovine respiratory disease complex. *Vet Microbiol* **170**, 58-64,
930 doi:10.1016/j.vetmic.2014.01.038 (2014).
- 931 67 Zhang, C., Habets, G. & Bollag, G. Interrogating the kinome. *Nat Biotechnol* **29**, 981-
932 983, doi:10.1038/nbt.2021 (2011).

- 933 68 Anastassiadis, T., Deacon, S. W., Devarajan, K., Ma, H. & Peterson, J. R.
934 Comprehensive assay of kinase catalytic activity reveals features of kinase inhibitor
935 selectivity. *Nat Biotechnol* **29**, 1039-1045, doi:10.1038/nbt.2017 (2011).
- 936 69 Davis, M. I. *et al.* Comprehensive analysis of kinase inhibitor selectivity. *Nat*
937 *Biotechnol* **29**, 1046-1051, doi:10.1038/nbt.1990 (2011).
- 938 70 Wu, Q. *et al.* Development of small molecule inhibitor-based fluorescent probes for
939 highly specific super-resolution imaging. *Nanoscale* **12**, 21591-21598,
940 doi:10.1039/d0nr05188h (2020).
- 941 71 Mohamed, A. J. *et al.* Bruton's tyrosine kinase (Btk): function, regulation, and
942 transformation with special emphasis on the PH domain. *Immunological Reviews*
943 **228**, 58-73, doi:<https://doi.org/10.1111/j.1600-065X.2008.00741.x> (2009).
- 944 72 Wang, X., Kokabee, L., Kokabee, M. & Conklin, D. S. Bruton's Tyrosine Kinase and
945 Its Isoforms in Cancer. *Front Cell Dev Biol* **9**, 668996, doi:10.3389/fcell.2021.668996
946 (2021).
- 947 73 Davids, M. S. & Brown, J. R. Ibrutinib: a first in class covalent inhibitor of Bruton's
948 tyrosine kinase. *Future Oncol* **10**, 957-967, doi:10.2217/fon.14.51 (2014).
- 949 74 Byrd, J. C. *et al.* Acalabrutinib (ACP-196) in Relapsed Chronic Lymphocytic
950 Leukemia. *N Engl J Med* **374**, 323-332, doi:10.1056/NEJMoa1509981 (2016).
- 951 75 Eierhoff, T., Hrinčius, E. R., Rescher, U., Ludwig, S. & Ehrhardt, C. The epidermal
952 growth factor receptor (EGFR) promotes uptake of influenza A viruses (IAV) into
953 host cells. *PLoS pathogens* **6**, e1001099-e1001099,
954 doi:10.1371/journal.ppat.1001099 (2010).

- 955 76 Bjorge, J. D. *et al.* Simultaneous siRNA Targeting of Src and Downstream Signaling
956 Molecules Inhibit Tumor Formation and Metastasis of a Human Model Breast
957 Cancer Cell Line. *PLOS ONE* **6**, e19309, doi:10.1371/journal.pone.0019309 (2011).
- 958 77 Bavagnoli, L. *et al.* The PDZ-ligand and Src-homology type 3 domains of epidemic
959 avian influenza virus NS1 protein modulate human Src kinase activity during viral
960 infection. *PloS one* **6**, e27789-e27789, doi:10.1371/journal.pone.0027789 (2011).
- 961 78 Hrinčius, E. R. *et al.* Avian influenza viruses inhibit the major cellular signalling
962 integrator c-Abl. *Cellular microbiology* **16**, 1854-1874, doi:10.1111/cmi.12332 (2014).
- 963 79 Hrinčius, E. R. *et al.* Nonstructural protein 1 (NS1)-mediated inhibition of c-Abl
964 results in acute lung injury and priming for bacterial co-infections: insights into 1918
965 H1N1 pandemic? *The Journal of infectious diseases* **211**, 1418-1428,
966 doi:10.1093/infdis/jiu609 (2015).
- 967 80 Ortiz, M. A. *et al.* Src family kinases, adaptor proteins and the actin cytoskeleton in
968 epithelial-to-mesenchymal transition. *Cell Commun Signal* **19**, 67,
969 doi:10.1186/s12964-021-00750-x (2021).
- 970 81 Vultur, A. *et al.* SKI-606 (bosutinib), a novel Src kinase inhibitor, suppresses
971 migration and invasion of human breast cancer cells. *Mol Cancer Ther* **7**, 1185-
972 1194, doi:10.1158/1535-7163.MCT-08-0126 (2008).
- 973 82 Hoffmann, H.-H., Palese, P. & Shaw, M. L. Modulation of influenza virus replication
974 by alteration of sodium ion transport and protein kinase C activity. *Antiviral research*
975 **80**, 124-134 (2008).
- 976 83 O'Brien, S. *et al.* FAK inhibition with small molecule inhibitor Y15 decreases viability,
977 clonogenicity, and cell attachment in thyroid cancer cell lines and synergizes with

978 targeted therapeutics. *Oncotarget* **5**, 7945-7959, doi:10.18632/oncotarget.2381
979 (2014).

980 84 Nimmerjahn, F. *et al.* Active NF-kappaB signalling is a prerequisite for influenza
981 virus infection. *J Gen Virol* **85**, 2347-2356, doi:10.1099/vir.0.79958-0 (2004).

982 85 Wurzer, W. J. *et al.* Caspase 3 activation is essential for efficient influenza virus
983 propagation. *EMBO J* **22**, 2717-2728, doi:10.1093/emboj/cdg279 (2003).

984 86 Wurzer, W. J. *et al.* NF-kappaB-dependent induction of tumor necrosis factor-related
985 apoptosis-inducing ligand (TRAIL) and Fas/FasL is crucial for efficient influenza virus
986 propagation. *J Biol Chem* **279**, 30931-30937, doi:10.1074/jbc.M403258200 (2004).

987 87 Jia, D. *et al.* Influenza virus non-structural protein 1 (NS1) disrupts interferon
988 signaling. *PLoS One* **5**, e13927, doi:10.1371/journal.pone.0013927 (2010).

989 88 Bozym, R. A. *et al.* Focal adhesion kinase is a component of antiviral RIG-I-like
990 receptor signaling. *Cell Host Microbe* **11**, 153-166, doi:10.1016/j.chom.2012.01.008
991 (2012).

992 89 Chapman, N. M., Connolly, S. F., Reinl, E. L. & Houtman, J. C. Focal adhesion
993 kinase negatively regulates Lck function downstream of the T cell antigen receptor.
994 *Journal of immunology* **191**, 6208-6221, doi:10.4049/jimmunol.1301587 (2013).

995 90 St-Pierre, J. & Ostergaard, H. L. A role for the protein tyrosine phosphatase CD45 in
996 macrophage adhesion through the regulation of paxillin degradation. *PLoS One* **8**,
997 e71531, doi:10.1371/journal.pone.0071531 (2013).

998 91 Park, S. Y. *et al.* Focal adhesion kinase regulates the localization and retention of
999 pro-B cells in bone marrow microenvironments. *Journal of immunology* **190**, 1094-
1000 1102, doi:10.4049/jimmunol.1202639 (2013).

- 1001 92 Ludwig, S. Disruption of virus-host cell interactions and cell signaling pathways as
1002 an anti-viral approach against influenza virus infections. *Biol Chem* **392**, 837-847,
1003 doi:10.1515/BC.2011.121 (2011).
- 1004 93 Gaur, P., Munjhal, A. & Lal, S. K. Influenza virus and cell signaling pathways. *Med*
1005 *Sci Monit* **17**, RA148-154, doi:10.12659/msm.881801 (2011).
- 1006 94 Roca Suarez, A. A., Van Renne, N., Baumert, T. F. & Lupberger, J. Viral
1007 manipulation of STAT3: Evade, exploit, and injure. *PLoS Pathog* **14**, e1006839,
1008 doi:10.1371/journal.ppat.1006839 (2018).
- 1009 95 Tsai, M. H., Pai, L. M. & Lee, C. K. Fine-Tuning of Type I Interferon Response by
1010 STAT3. *Front Immunol* **10**, 1448, doi:10.3389/fimmu.2019.01448 (2019).
- 1011 96 Guo, L., Wang, Q. & Zhang, D. MicroRNA-4485 ameliorates severe influenza
1012 pneumonia via inhibition of the STAT3/PI3K/AKT signaling pathway. *Oncol Lett* **20**,
1013 215, doi:10.3892/ol.2020.12078 (2020).
- 1014 97 Hui, K. P. *et al.* Highly pathogenic avian influenza H5N1 virus delays apoptotic
1015 responses via activation of STAT3. *Sci Rep* **6**, 28593, doi:10.1038/srep28593
1016 (2016).
- 1017 98 Shi, C. S. & Kehrl, J. H. Pyk2 amplifies epidermal growth factor and c-Src-induced
1018 Stat3 activation. *J Biol Chem* **279**, 17224-17231, doi:10.1074/jbc.M311875200
1019 (2004).
- 1020 99 REED, L. J. & MUENCH, H. A SIMPLE METHOD OF ESTIMATING FIFTY PER
1021 CENT ENDPOINTS¹². *American Journal of Epidemiology* **27**, 493-497,
1022 doi:10.1093/oxfordjournals.aje.a118408 (1938).

1023 100 Grishagin, I. V. Automatic cell counting with ImageJ. *Anal Biochem* **473**, 63-65,

1024 doi:10.1016/j.ab.2014.12.007 (2015).

1025

1026

1027 **FIGURE LEGENDS**

1028 **Figure 1.** Main target specificity of candidate NRTKIs used in this study.

1029

1030 **Figure 2:** Effect of SMKI treatment on NL09 and NL11 replication at MOI 1. A549 cells
1031 were infected with pandemic H1N1 strain NL09 and seasonal H3N2 strain NL11 at MOI1
1032 and incubated for 72h in the presence of SMKI concentrations of 0.25x, 0.5x and 1x with
1033 1x being the highest non-toxic concentration under infection conditions (Tab. 1). At 24,
1034 48, and 72 hpi, supernatants were collected and viral titers quantified by TCID₅₀/ml assay
1035 (n = 4). Means ±SD are shown. *, P<0.05; **, P<0.01; ***, P<0.001; ****, P<0.0001; ns,
1036 not significant (P>0.05).

1037

1038 **Figure 3.** NRTKIs effects on cell viability and infectivity during infection. A549 cells were
1039 infected with pandemic H1N1 strain (NL09) and seasonal H3N2 strain (NL11) (MOI=1)
1040 and incubated in the presence of SMKIs (0.5x of the highest non-toxic concentration) for
1041 48h. A) Fluorescence microscopy pictures were captured using a Leica DMI8
1042 fluorescence microscope (representative field shown from an n=4/condition). Virus-
1043 infected cells were detected by anti-IAV NP antibody (red), and nuclei were detected
1044 using NucBlue Live ReadyProbes (blue). B) Heatmap visualization of NRTKIs affect cell
1045 viability (blue/green) and infectivity (red) relative to untreated infection in A549 cells.
1046 Images were quantified using ImageJ software suite. Data is based all fields represented
1047 in (A) (n=4/condition).

1048

1049 **Figure 4.** MOI-independent effect of NRTKIs on IAV infection. A549 cells were infected
1050 with pandemic H1N1 strain (NL09) and seasonal H3N2 strain (NL11) at either (MOI=0.1
1051 or 3) and incubated for 72h in the presence of NRTKIs at 0.25x (gray) and 0.5x (white) of
1052 highest-toxic concentrations. At 24, 48, and 72 hpi, supernatants were collected and viral
1053 titers quantified by TCID₅₀/ml assay (n=4). Means ±SD are shown. *, P<0.05; **, P<0.01;
1054 ***, P<0.001; ****, P<0.0001; ns, not significant (P>0.05).

1055
1056 **Figure 5.** Effect of NRTKI treatment on *ex vivo* IAV infection. A) hPCLS were infected
1057 with pandemic H1N1 strain (NL09) and seasonal H3N2 strain (NL11) at increasing doses
1058 (10⁴, 10⁵ and 10⁶ TCID₅₀/200 ul). At 2, 16, 24, 48, 72, 96, and 144 hpi culture supernatants
1059 were sampled and viral titers quantified by TCID₅₀/ml assay. The supernatants were
1060 replenished after collection at every time point (8 donors; n=24/virus); means ±SEM are
1061 shown. B) Heatmap visualization of NRTKI cytotoxicity based on LDH release of hPCLS
1062 normalized to DMSO control, and relative to 1% Triton-X 100 treated cells; NRTKIs were
1063 treated with 1x and 10x of highest cytotoxic concentration on A549 cells (Fig. 1) for up to
1064 144h. At every time point, LDH release was determined using LDH-Glo Cell Viability
1065 Assay (8 donors / n=24). C) PCLS were infected with NL09 or NL11 (10⁵ TCID₅₀ / 200 ul)
1066 and incubated for 120h in the presence of NRTKIs (Defactinib 50uM; Acalabrutinib 5uM;
1067 Ibrutinib 5uM; Bosutinib 5uM; Nilotinib 10uM; Saracatinib 0.125uM). Growth curves from
1068 supernatants collected at 2, 12, 24, 48, 72, and 120 hpi were quantified by TCID₅₀/ml
1069 assay (3 donors; n=6/condition); means ±SEM are shown. D) NL11 infected hPCLS were
1070 fixed 120 hpi and the PFA-fixed paraffin-embedded (PFPE) PCLS were were cut into 2
1071 μm thick section. Shown is H&E staining and viral anti-NP immunohistochemical staining

1072 (brown). Original magnification 10x. E) Semi-quantitative analysis of virus infected (anti-
1073 NP staining) was performed for all tested NRTKIs using FIJI image-analysis software
1074 platform and normalized to whole section areas.

1075

1076 **Figure 6.** Stability of NRTKI treatment effect. (A) Effect of SMKI treatment on NL09 and
1077 NL11 replication at MOI=0.001 over serial passages was determined by growth curves
1078 using MDCK cells infected with pandemic H1N1 strain (NL09) or seasonal H3N2 strain
1079 (NL11) at MOI=0.001 and incubated for 72h in the presence of the highest non-toxic
1080 NRTKI concentrations (n=2). At 72 hpi, samples were collected, and viral titers were
1081 assessed by TCID₅₀/ml assay on MDCK cells (n = 4). MDCK cells were infected as before
1082 at MOI=0.001 according to the assessed viral titers. Means ±SD are shown. (B) NL09
1083 and NL11 virus stocks were pre-incubated with control (DMSO) or the 1x concentration
1084 of the respective NRTKI for 4h at 37°C. A549 cells were then infected using a 1:1000
1085 dilution of the NRTKI pre-incubated virus stocks and incubated for 72h. At 72 hpi, samples
1086 were collected, and viral titers were assessed by TCID₅₀/ml assay (n=3). Means ±SD are
1087 shown. *, P<0.05; **, P<0.01; ***, P<0.001; ****, P<0.0001; ns, not significant (P>0.05).

1088

1089 **Figure 7.** The effect of NRTKI on viral entry. A549 cells were pretreated with NRTKIs for
1090 2h and then infected with the NL09 and NL11 strains (MOI=10) for 0.5h in the presence
1091 or absence of the inhibitors. The cells were fixed and permeabilized. Virions were
1092 detected by anti-NP (green) antibody, F-Actin was detected by ActinRed-555 (red), and
1093 nuclei were detected using NucBlue Live ReadyProbes (blue). and virion localization was
1094 assessed by confocal microscopy using a 63x oil immersion objective (n = 2).

1095

1096 **Figure 8.** NRTKIs effects on IAV RNA replication. (A) A549 cells were transfected with
1097 pPOLI-358-FFluc and pmaxGFP plasmids. At 24 hpt, cells were either infected with NL09
1098 or NL11 at MOI=1 in the presence or absence of indicated NRTKIs. At 48 hpt (24 hpi),
1099 luciferase activity was measured and normalized to GFP expression (MFI). (B) A549 cells
1100 were transfected with pPOLI-358-FFluc and pmaxGFP plasmids and co-transfected with
1101 either NL09 or NL03-minigenome plasmids. At 6 hpt, the indicated NRTKIs were added
1102 to the medium. At 30 hpt (24 h of treatment), luciferase activity was measured and
1103 normalized to GFP MFI. Bars indicate values relative to infected untreated cells
1104 normalized to GFP. For each system luminescence of untreated infected A549 cells
1105 relative to GFP displays the replication kinetics of the respective polymerase complex. All
1106 measurements were taken in triplicates from triplicate samples (n=3). Error bars indicate
1107 \pm standard deviation (SD). *, P<0.05; **, P<0.01; ***, P<0.001; ****, P<0.0001; ns, not
1108 significant (P>0.05). P-values determined by Brown-Forsythe and Welsh ANOVA
1109 compared to untreated.

1110

1111 **Figure 9.** Effect of NRTKIs treatment on STAT3 activation. A549 cells were infected with
1112 NL09 (A) or NL11 (B) at MOI=1. Total proteins were isolated from whole cell lysate at 18
1113 and 48 hpi and immunoblot assay was performed for phospho- and total STAT3, IAV-NP
1114 and bActin. Chemiluminescence was detected and quantified using the Li-Cor C-DiGit
1115 and Image Studio 5.1 CLX software. All measurements were taken from two western blots
1116 from two independent experiments (n=2). All values are relative to untreated virus-
1117 infected cells. P=phosphor, T=total. Error bars indicate \pm standard deviation (SD). *,

1118 P<0.05; **, P<0.01; ***, P<0.001; ****, P<0.0001; ns, not significant (P>0.05). P-values
1119 determined by students t-test compared to untreated virus-infected cells.

1120

1121 **Figure 10.** Effect of NRTKIs on NFkB activation. A549 cells were infected with NL09 (A)
1122 or NL11 (B) at MOI=1. Protein was isolated from whole cell lysate at 18 and 48 hpi and
1123 immunoblot assay was performed for pNFkB p65, panNFkB p65, IAV NP and bActin.
1124 Detected signal was quantified using the Li-Cor C-DiGit and Image Studio 5.1 CLX
1125 software. (C) NL09, NL11 or mock infected cells were treated with poly(IC) at
1126 concentrations of 50 ng/ml and 200 ng/ml. Total proteins were isolated from whole cell
1127 lysate at 18 and 48 hpi and immunoblot assay was performed for phospho- and total
1128 NFkBp65, IAV NP and bActin. All measurements were taken from two western blots from
1129 two independent experiments (n=2). All values are normalized to bActin and relative to
1130 untreated of the respective time-point. Error bars indicate \pm standard deviation (SD).
1131 P=phosphorylated and T=total. *, P<0.05; **, P<0.01; ***, P<0.001; ****, P<0.0001; ns,
1132 not significant (P>0.05). P-values determined by students t-test compared to untreated
1133 virus infected cells.

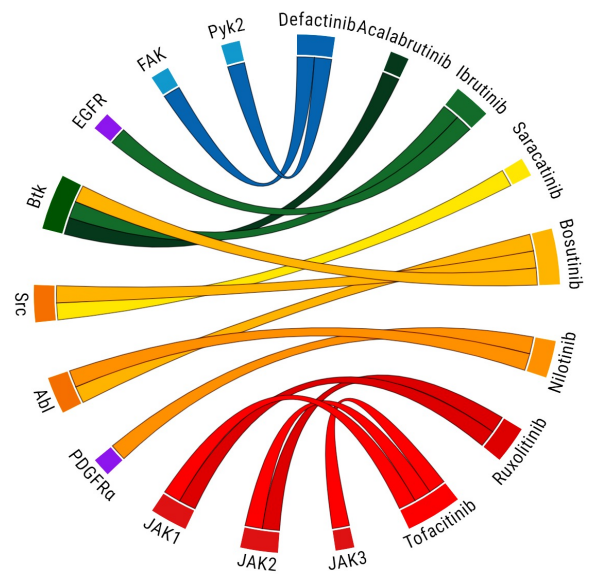
1134

Table 1. Main targets of FDA-approved NRTKIs used

NRTKIs	Main target	1x dose (μM)	FDA approved conc. (μM)*	Reference(s)
Defactinib (VS-6063)	FAK, Pyk2	5	1.26**	[47]
Acalabrutinib (ACP-196)	Btk	0.5	0.69	[43, 44]
Ibrutinib (PCI-32765)	Btk, EGFR	0.5	2.05	[45, 46]
Bosutinib (SKI-606)	Abl, Src, Btk	5	1.82	[40, 41]
Nilotinib (AMN-107)	Abl, PDGFRα	1	2.44	[38, 39]
Saracatinib (AZD0530)	Src	0.125	0.37	[42]
Ruxolitinib (INCB018424)	JAK1/2	5	0.21	[37]
Tofacitinib (CP-690550)	JAK1/2/3	10	0.1	[36]

* FDA approved concentrations calculated from orally administered dosage per 24h based on average adult person's weight according to WHO (62.0kg).

** Defactinib FDA-approved concentration based on dosage information of orphan drug clinical studies.



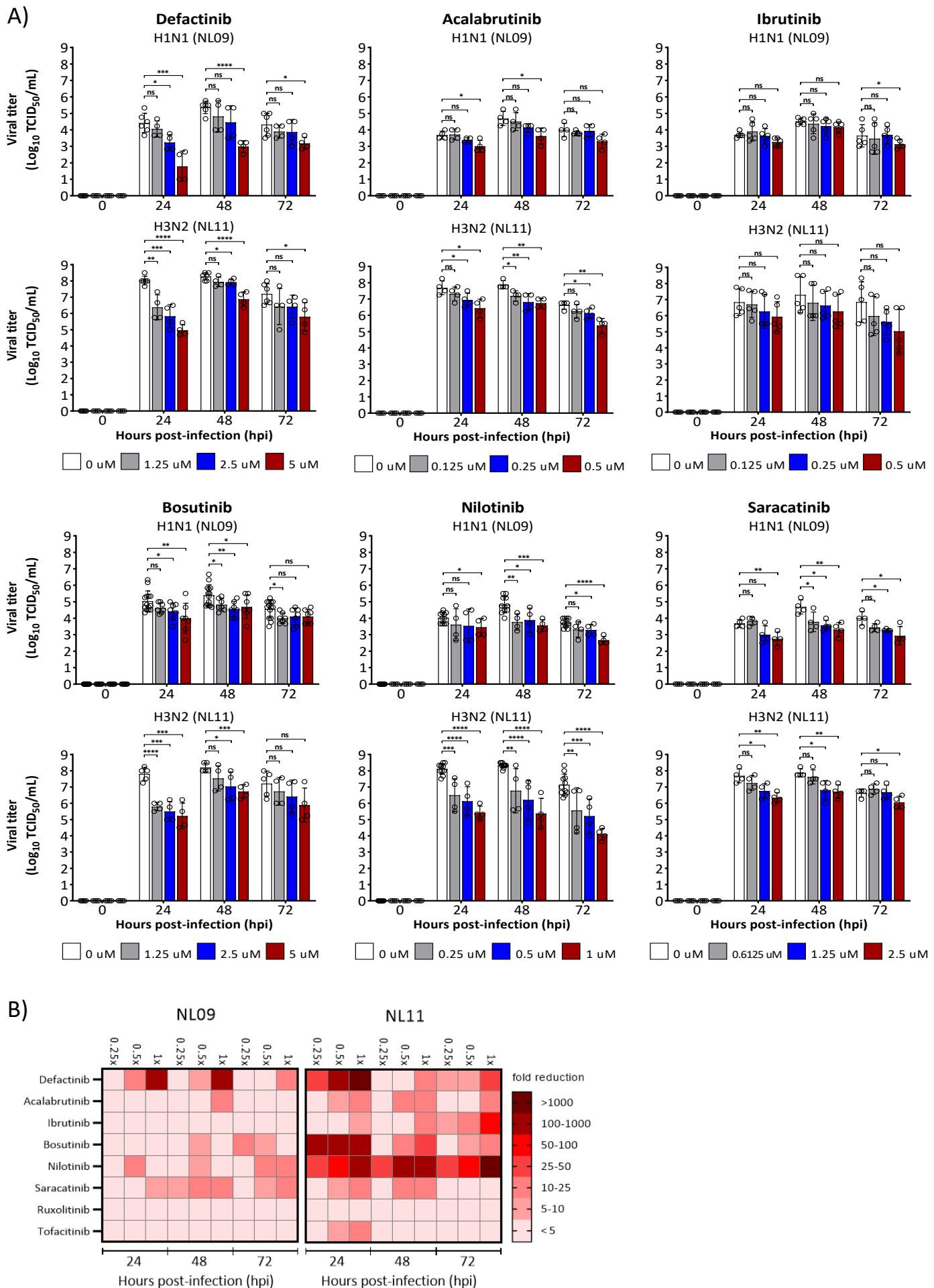


Figure 2

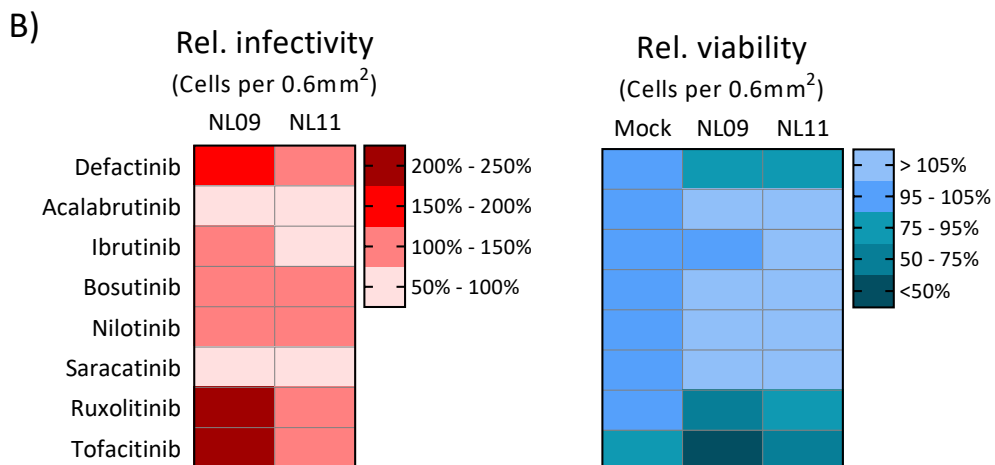
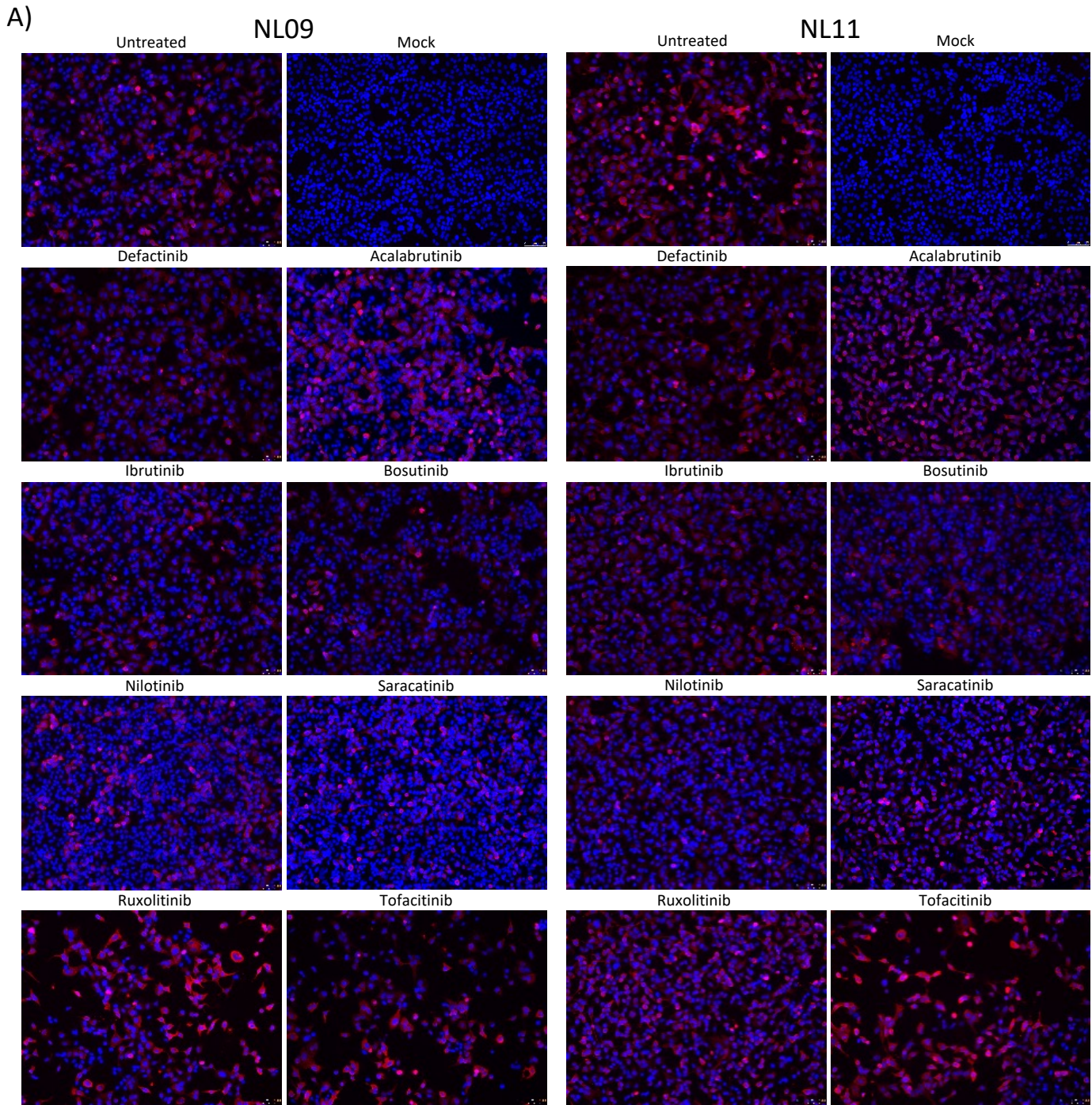


Figure 3

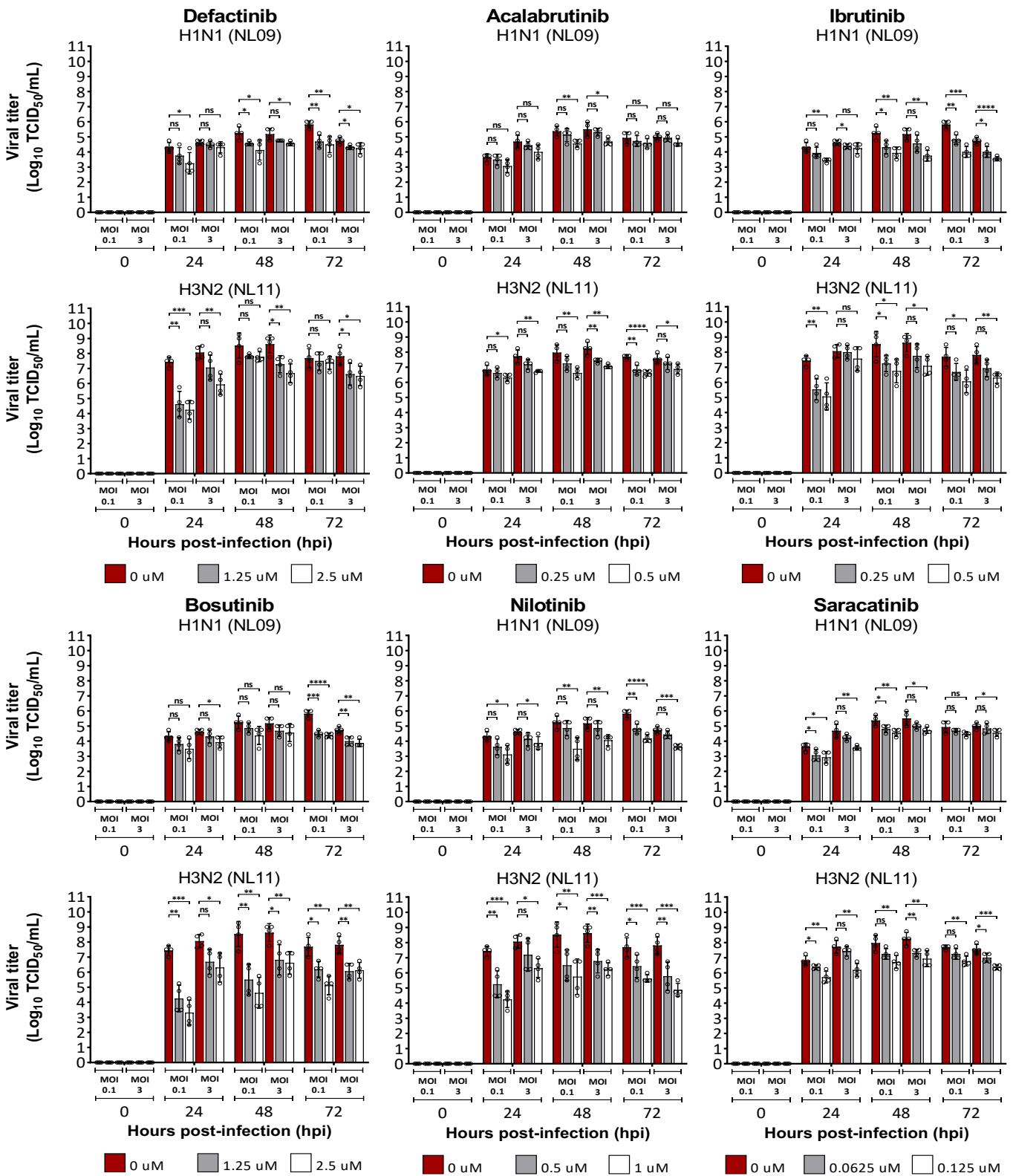
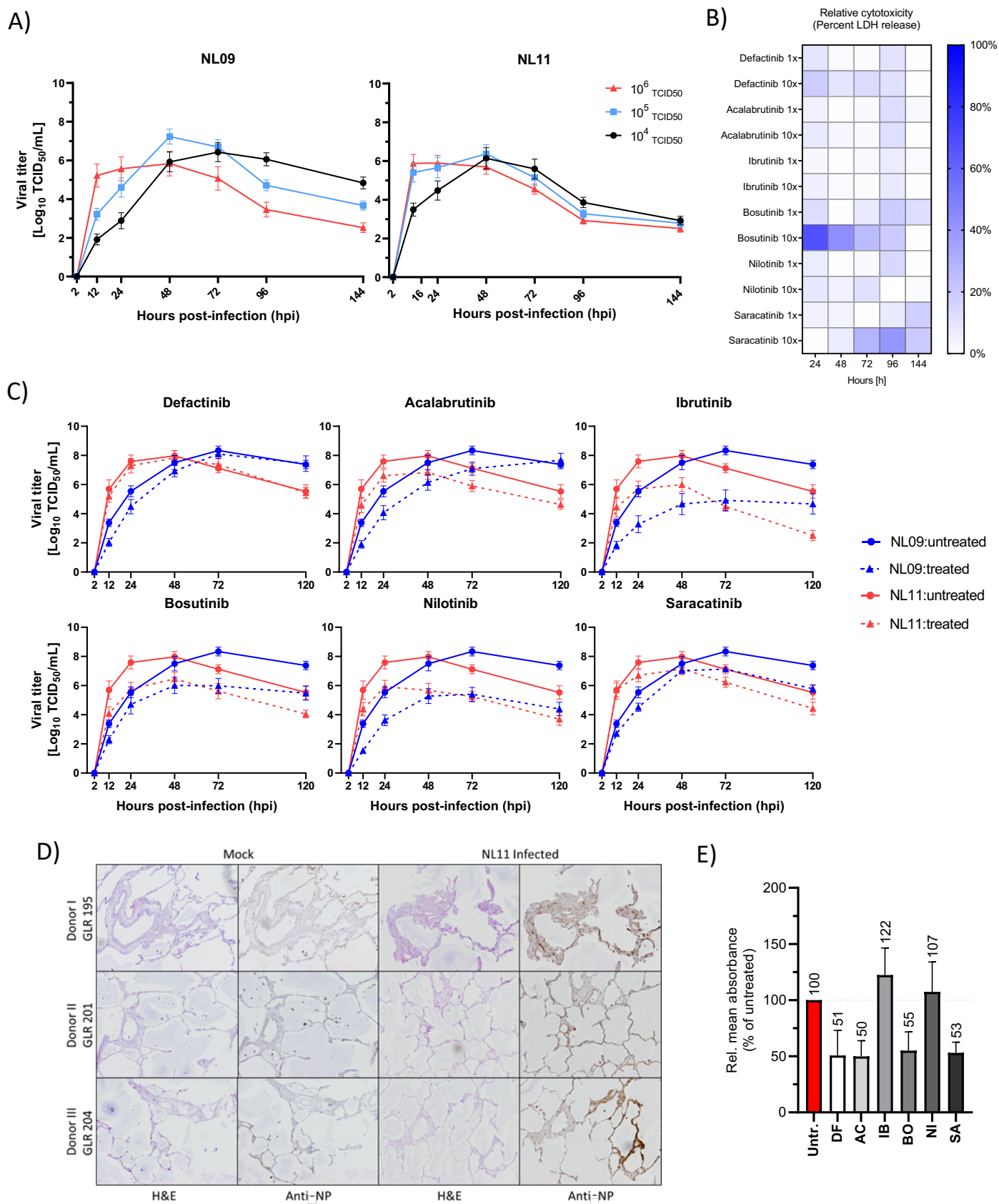


Figure 4



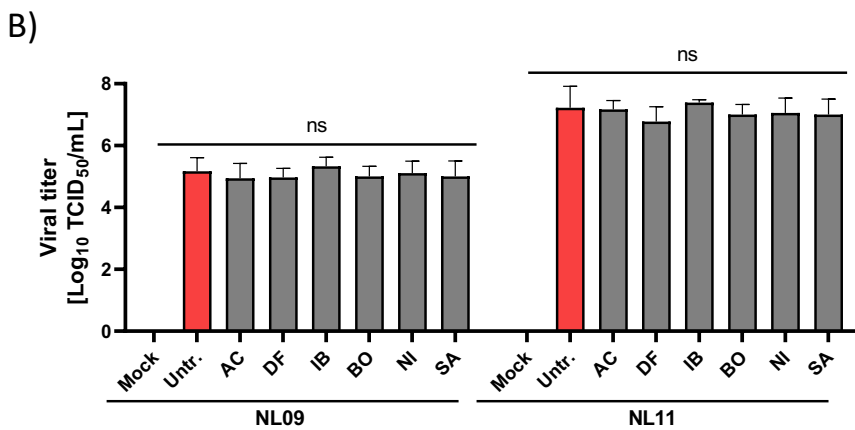
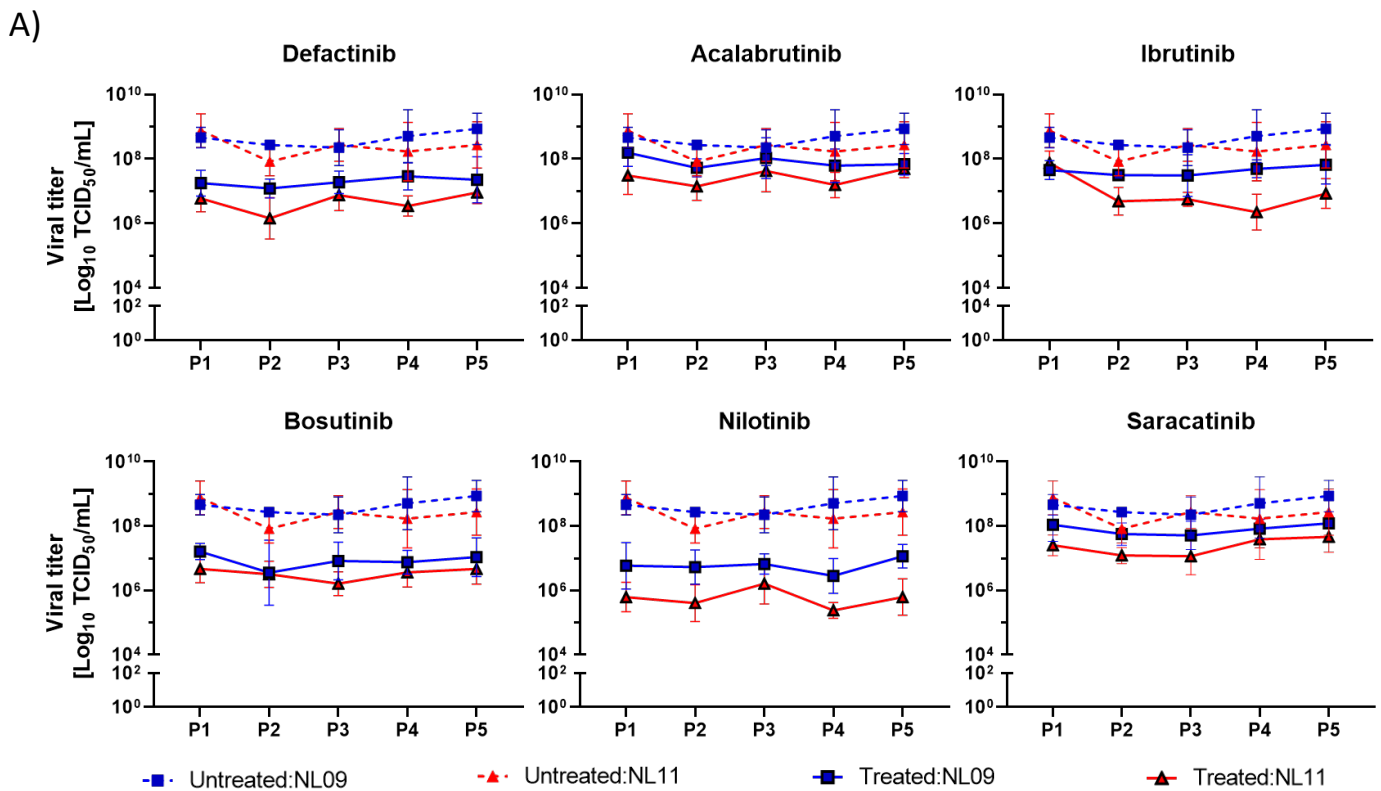


Figure 6

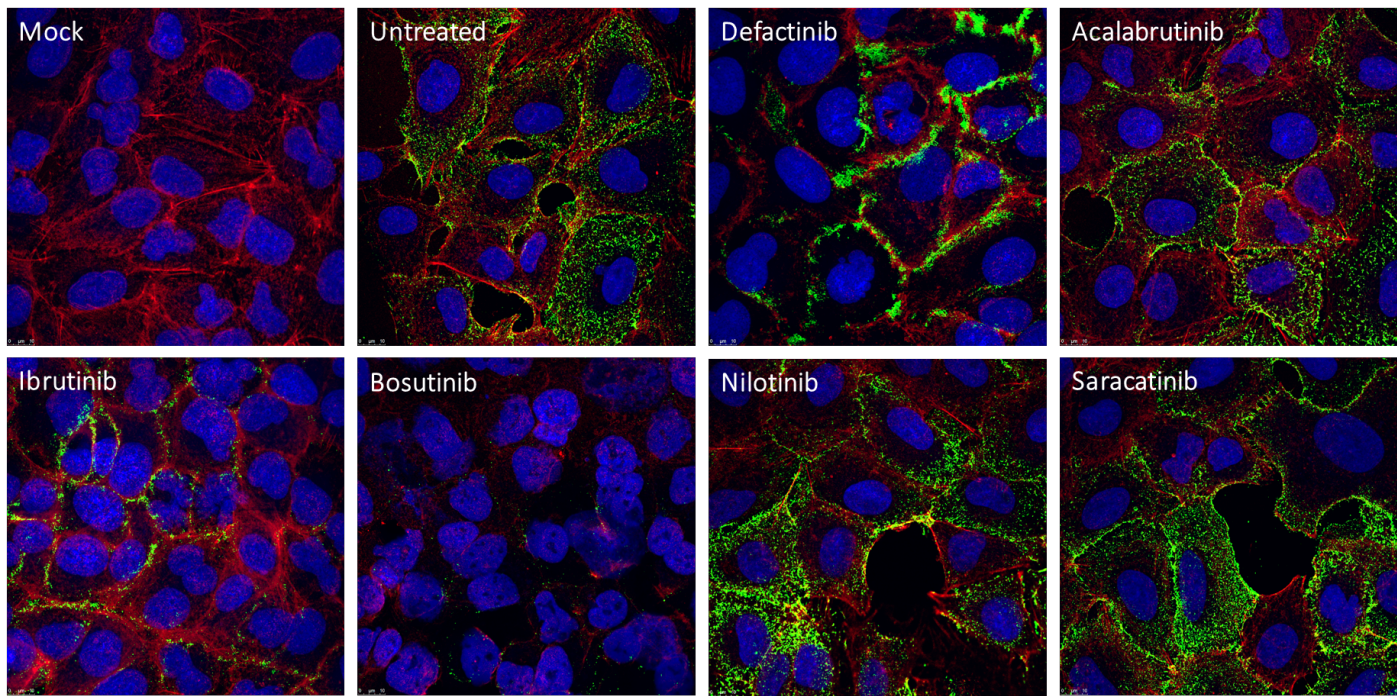


Figure 7

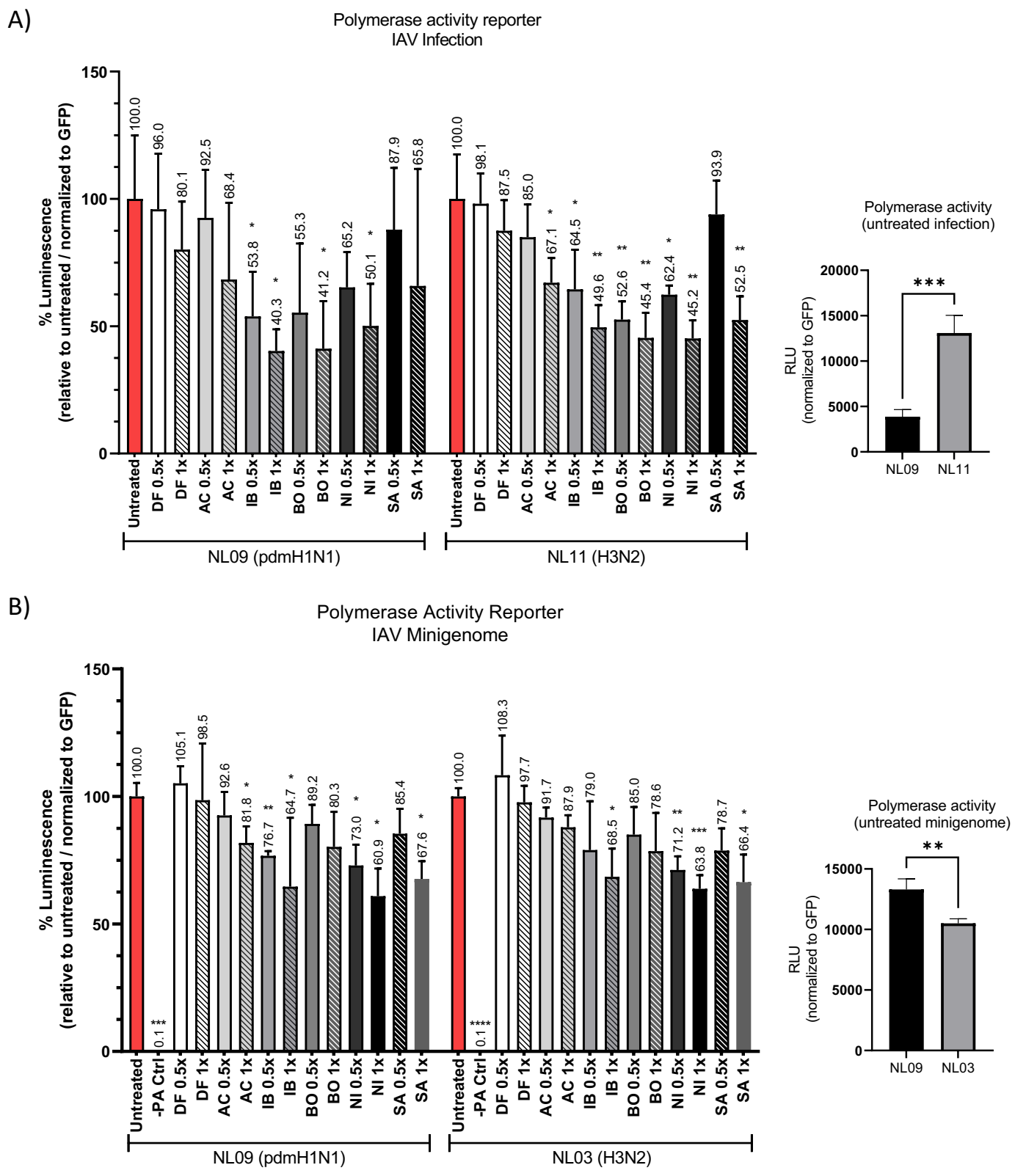


Figure 8

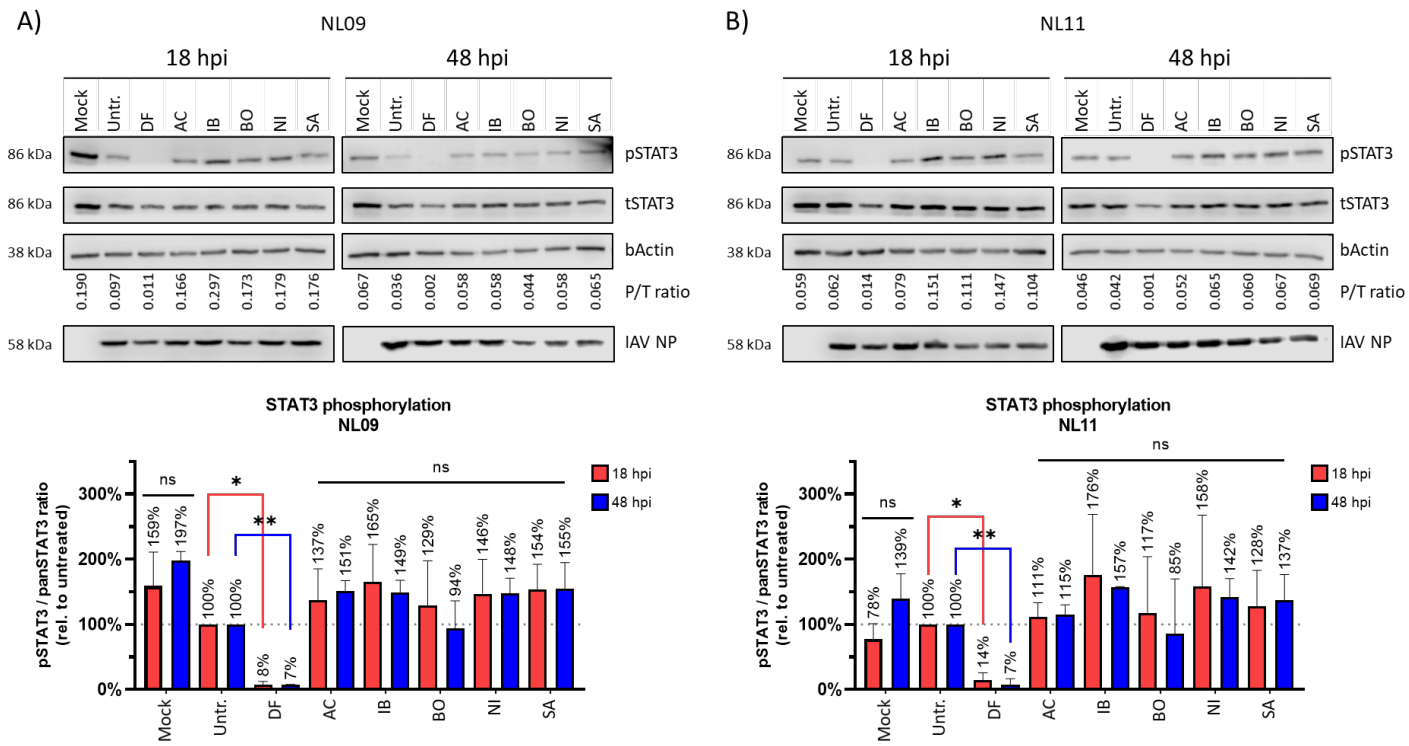


Figure 9

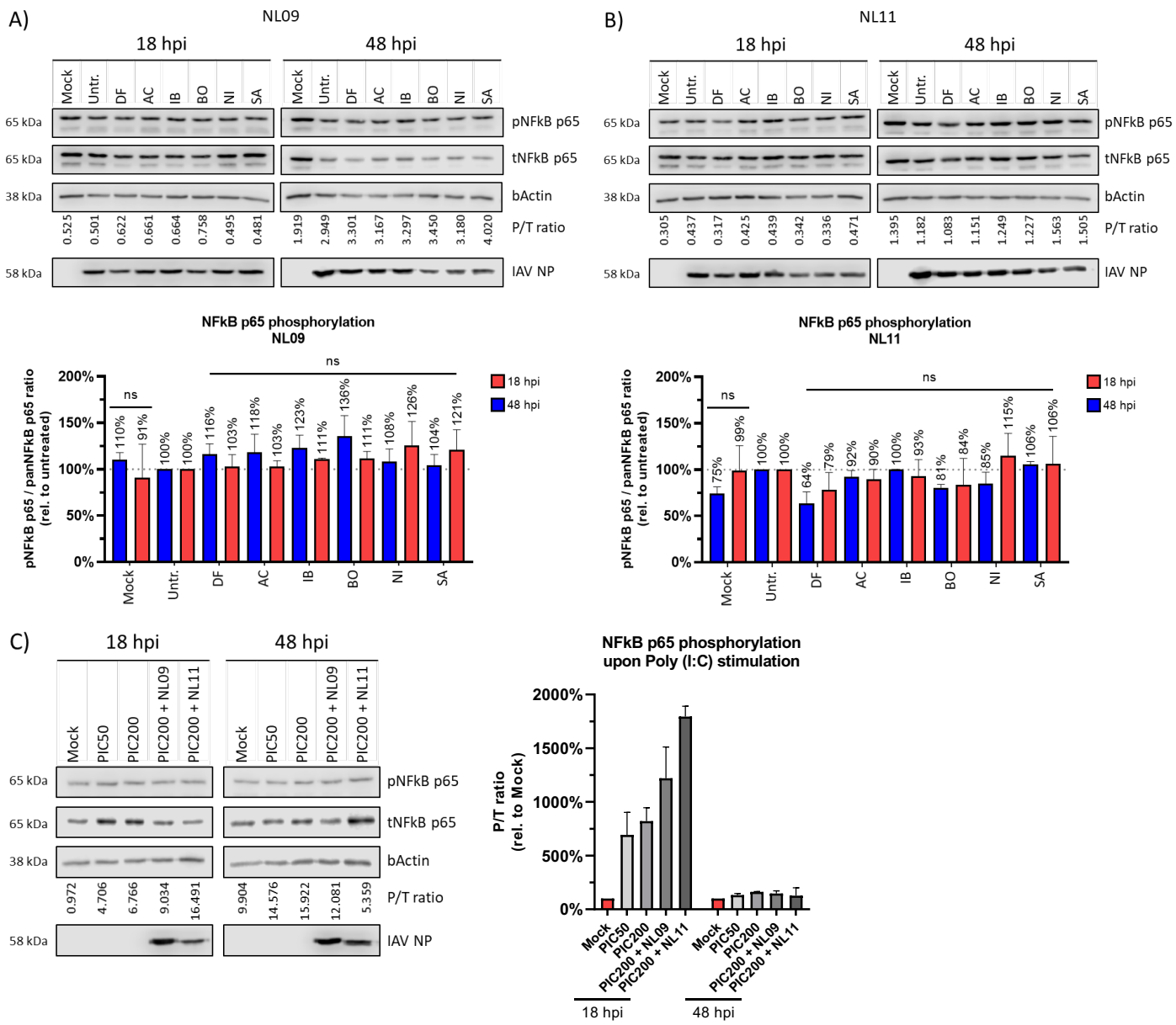


Figure 10